

Fall 2006

Exchange Hydrodynamics Between a Subestuary and Its Adjacent Estuary

Diego A. Narváez
Old Dominion University

Follow this and additional works at: https://digitalcommons.odu.edu/oeas_etds



Part of the [Oceanography Commons](#)

Recommended Citation

Narváez, Diego A.. "Exchange Hydrodynamics Between a Subestuary and Its Adjacent Estuary" (2006).
Master of Science (MS), Thesis, Ocean & Earth Sciences, Old Dominion University, DOI: 10.25777/
za48-3m34
https://digitalcommons.odu.edu/oeas_etds/268

This Thesis is brought to you for free and open access by the Ocean & Earth Sciences at ODU Digital Commons. It has been accepted for inclusion in OES Theses and Dissertations by an authorized administrator of ODU Digital Commons. For more information, please contact digitalcommons@odu.edu.

**EXCHANGE HYDRODYNAMICS BETWEEN A SUBESTUARY
AND ITS ADJACENT ESTUARY**

by

Diego A. Narváez
B. S. December 2000, Pontificia Universidad Católica de Valparaíso

A Thesis Submitted to the Faculty of
Old Dominion University in Partial Fulfillment of the
Requirement for the Degree of

MASTER OF SCIENCE

OCEAN AND EARTH SCIENCE

OLD DOMINION UNIVERSITY
December 2006

Approved by:

Larry P. Atkinson (Director)

Chester E. Grosch (Member)

John M. Klinck (Member)

Arnoldo Valle-Levinson (Member)

ABSTRACT

EXCHANGE HYDRODYNAMICS BETWEEN A SUBESTUARY AND ITS ADJACENT ESTUARY

Diego A. Narváez
Old Dominion University, 2006
Director: Dr. Larry P. Atkinson

Four oceanographic surveys and two periods of moored data were analyzed to describe the subtidal exchange hydrodynamics between a subestuary (Nansemond River) and its adjacent estuary (James River) in the lower Chesapeake Bay. The surveys were carried out during two semidiurnal periods (~25 hrs), which included two spring and two neap tides. Velocity profiles and hydrographic data were recorded over an area ~4 km long and ~1 km wide allowing a spatial resolution rarely obtained with observational data. The results obtained in the surveys were extended with instruments deployed at the entrance to the subestuary during winter and summer time (~80 days for each deployment). The combination of both data sets allowed a comprehensive characterization of the main factors driving the subtidal circulation. The circulation pattern observed in the subestuary is caused primarily by the interaction between local topography and winds. Buoyancy forcing, Earth's rotation and centripetal accelerations are secondary factors. The curved funnel shape of the lower subestuary favors a subtidal recirculation. This recirculation is enhanced by an adverse pressure gradient and by westward wind, which drives inflow over the shallow parts and outflow in the channel. The adverse pressure gradient is caused by intrusion of low-salinity waters through the shoals of the subestuary, especially during episodic increases of river discharge at the estuary. The subestuary's transverse partition of the wind-induced circulation shows

good agreement with previous results obtained mainly with analytical and numerical models. Thus, the observational data presented in this research are among the few to validate such numerical results.

Copyright, 2006, by Diego A. Narváez, All Rights Reserved.

To my family.....Andrea and Luna

ACKNOWLEDGMENTS

I would like to thank my advisor Dr. Arnaldo Valle-Levinson for giving me the chance to start a graduate program and show me the interesting world of estuaries. Also I want to especially thank Dr. Larry Atkinson for being my “forced” substitute advisor. Also I gratefully acknowledge Dr. Chester Grosch and Dr. John Klinck for being part of my thesis committee. Thanks to the U.S National Science Foundation (NSF), under grants 9983685 and 0425147, for funding me and this study. The support of ONR award N000140510829 is also greatly appreciated during the last semester in the graduate program. I also want to extend my gratitude to the staff and faculty members of CCPO and OEAS for their support and help. Finally thanks to all the students and staff who participated during the long and arduous collection of the data used in this thesis.

TABLE OF CONTENTS

	Page
ABSTRACT.....	ii
COPYRIGHT.....	iv
DEDICATION.....	v
ACKNOWLEDGMENTS	vi
LIST OF TABLES.....	viii
LIST OF FIGURES	ix
 CHAPTER	
1. INTRODUCTION	1
2. STUDY AREA	5
3. DATA COLLECTION AND PROCESSING	8
4. RESULTS	12
4.1 Oceanographic Surveys	12
4.1.1 Atmospheric and Hydrographic Conditions	12
4.1.2 Subtidal Circulation	14
4.1.3 Volume Flux Estimations	20
4.2 Temporal Variability	24
4.2.1 Time Domain Analysis.....	24
4.2.2 Frequency Domain Analysis.....	29
4.2.3 Empirical Orthogonal Functions	36
5. DISCUSSION.....	39
6. CONCLUSION.....	47
REFERENCES	48
VITA.....	53

LIST OF TABLES

Table	Page
1. Estimations of Mean Volume Fluxes Separated by Survey and Transects.	21
2. Volume Fluxes (Q_{est}) and Velocity Estimations (V_{est}) for Outflows and Inflows through the Area not Covered During the Data Collection.	22
3. Wind Statistics for Winter and Summer Deployments, Units are in $m\ s^{-1}$	27
4. Percentage Explained for the First Three EOF Modes for Each Deployments and Location at the Entrance of the Nansemond River.	36
5. Momentum Equation Scaling During Each Cruise for T1.....	40
6. Baroclinic Pressure Gradients Estimated with Available CTD Data.....	41

LIST OF FIGURES

Figure	Page
1. Map of the Study Area at the Nansemond River Estuary in the Lower Chesapeake Bay.....	6
2. Time Series of Wind (a-b) and River Discharge (c-d) for Each Survey.	13
3. Mean Horizontal Surface Salinity Fields and Mean Salinity Profiles During N1 (a,b), N2 (c,d), N3 (e,f), and N4 (g,h).....	14
4. Subtidal Flow at T1 During N1 (a), N2 (b), N3 (c) and N4 (d).....	15
5. Same as Fig. 4 but for Subtidal Flow at T2	16
6. Same as Fig. 4 but for Subtidal Flow at T3	17
7. Mean Velocity Profile for Each Survey in the Channel at T1 (a,d), T2 (b,e) and T3 (c,f).	18
8. Horizontal Currents Field for N1, N2, N3 and N4 (a, b, c, d, respectively).....	19
9. Times Series for the Winter Deployment.	25
10. Times Series for the Summer Deployment	28
11. Spectral Analysis for James River Discharge and Bottom Salinity in the Subestuary for Winter Deployment.	30
12. Currents, Wind and Sea Level Spectral Analysis for Winter Deployment	31
13. Same as Fig. 12 but for Summer Deployment	32
14. Coherence and Phase Spectra between Along-Estuary Wind and Sea Level at Sewells Point (SP) and Bottom Pressure in the Channel (C) and Over the Shoal (S) for (a,b) Winter and (c,d) Summer Deployments	33
15. Coherence Spectra Contours Between: Winter Along-channel Flow in the Channel and, (a) Along-Estuary Wind, (b) Bottom Pressure in the Channel.....	34
16. Same as Fig. 15 but for Phase Spectra	35
17. First Mode of Empirical Orthogonal Functions (EOF) of (a) Winter and (c) Summer Deployment.....	37

Figure	Page
18. Second Mode of EOF for: Winter, (a) Channel and (b) Shoals.....	38
19. Hypothetical Representation of (a) Bernoulli Circulation in a Simple Funnel, (b) Circulation in an Estuary-Like Funnel, and (c) the Circulation Pattern Observed in this Study as a Result of a Curved Funnel Shape of the Subestuary	42

CHAPTER 1

INTRODUCTION

An estuarine system is an area where river waters interact with the coastal ocean. In this area a so-called estuarine circulation can be explained in terms of density gradients driven by salinity differences between river and coastal waters. As a result relatively light river flow tends to run out of the estuary along the surface layer, while dense salty waters run into the estuary along the bottom layer due to mass conservation. However, factors like tides, wind, the interaction of local bathymetry with wind, friction and Earth's rotation, can modify this simple model of water exchange (see Uncles, 2002 for a review).

The major influence of tides over the subtidal estuarine circulation occurs at fortnightly scales (~14 days), i.e., spring and neap tides. The effects are seen as intensification of the estuarine circulation during neap tides and attenuation during spring tides (e.g. Haas, 1977; Nunes and Lennon, 1987; Simpson et al., 1990; Valle-Levinson et al., 2000). In neap tides, slow tidal flows result in weak tidal straining and reduced vertical mixing. Hence, the river outflow and ocean inflow are better developed than in spring tides because of the well-defined pycnocline between the surface and the bottom layer. During spring tides, tidal currents are stronger than in neap tides causing an increase in vertical mixing. This results in attenuation of the estuarine circulation.

Wind also is a mechanism that modifies estuarine circulation and the volume exchange that occurs between the estuary and the adjacent coastal ocean. Subtidal wind-induced exchange has received attention in the past decades, especially the influence of

local and remote wind (e.g., Garvine, 1985; Valle-Levinson and Atkinson, 1999; Wong and Valle-Levinson, 2002; Wong, 2002; Sanay and Valle-Levinson, 2005).

Remote wind can produce a rise/drop of the sea level that propagates to the entrance of an estuary. If sea level set-up occurs, a unidirectional barotropic inflow is expected at the entrance of the estuary while a set-down can produce a barotropic outflow (Wong, 1994). On the other hand, local wind tends to produce a bidirectional flow: while the direction of surface currents is the same as that of the wind, the near bottom current flows in opposite direction (Officer, 1976; Wang, 1979a; Wong and Valle-Levinson, 2002). From a temporal point of view, winds and sea levels in coastal areas are dominated by fluctuations with period of ~3-7 days (Wong and Garvine, 1984). High coherence among wind, sea level and subtidal circulation has been found at those periods (Wong, 2002).

Many estuaries show complex transverse bathymetries, for example, channels flanked by shoals. The interaction of this type of bathymetry with winds, friction and Earth's rotation might modify the subtidal estuarine circulation in different ways. In some estuaries dominated by density gradients, this interaction results in inflows mainly in channels and outflows over shoals (e.g., Wong, 1994; Kasai et al., 2000; Valle-Levinson et al., 2003). In other estuaries dominated by tidal forcing, the subtidal flow can be the opposite, i.e., inflows over shoals and outflows in channels (e.g., Li and O'Donnell, 1997). Furthermore, local winds might produce downwind flows over shoals and upwind flows in channels (Wong, 1994; Winant, 2004; Sanay and Valle-Levinson, 2005). Under strong frictional effects both the inflow in channels and the outflow over shoals occur throughout the water column (Wong, 1994; Friedrichs and Hamrick, 1996). When the

frictional effect is weak the inflows appear only in the bottom layer in the channel and outflows are found at the surface in the channel and over the entire shoals (Kasai et al., 2000; Valle-Levinson et al., 2003). Earth's rotation and the changes of local topography along the estuary also influences the lateral variability of the subtidal flow (Valle-Levinson and O'Donnell, 1996; Valle-Levinson et al., 2000; Geyer 1993). Outflows tend to tilt to the left (looking into the estuary in the Northern Hemisphere) in estuaries where Earth's rotation is important (Valle-Levinson and O'Donnell, 1996). Geyer (1993) showed that curved estuaries or channels might induce centrifugal accelerations forming secondary or lateral circulation near the curvature. In addition the lateral circulation increases near the head of the estuary producing an area of flow return (Sanay and Valle-Levinson, 2005)

Although all the information presented above shows that the estuarine circulation and its modifications have been well documented, most of this knowledge has been acquired in the interaction area of estuaries and adjacent coastal oceans or in the estuary proper. However, less attention has been paid to small tributaries (or subestuaries) of relatively large estuaries located close to areas with great human impact. Here salinity gradients still allow formation of estuarine circulation but the gradients can reverse under large river discharge entering the large estuary. The effects of these changes in salinity patterns can induce reversal of estuarine circulation as have been found for some coastal lagoons (Valle-Levinson et al., 2001).

Additionally, in view of the vast area covered by large estuaries, observational data with good spatial resolution have been rarely obtained. Thus most of the spatial and vertical features in the estuarine circulation have been studied mainly with numerical and

analytical models. These models have shown well-developed transverse partition of the wind-induced outflows and inflows (Wong, 1994; Winant, 2004; Shen et al., 1999; Chen et al., 2003). Also, these studies have shown complex horizontal patterns, like recirculation areas or eddies (Shen et al., 1999; Chen et al., 2003). Observational data are required to complement such modeling efforts.

The ultimate objective of this work is to advance the understanding of the subtidal exchange that occurs between a small estuary or subestuary (Nansemond River) and its adjacent estuary (James River). To address this objective three specific objectives are proposed:

- (1) Determine the spatial and vertical structure of the estuarine circulation in the study area.
- (2) Determine the influence of the estuary on the subtidal exchange in the subestuary.
- (3) Evaluate the influence of tides, winds, and local topography on the subtidal exchange between the subestuary and its adjacent estuary.

CHAPTER 2

STUDY AREA

The study area is the Nansemond River subestuary, a tributary of the James River estuary located in the lower Chesapeake Bay (Fig. 1). The Nansemond River is a semi-enclosed system with no known gauged freshwater input. Its freshwater sources come from rainfall and sewer discharges from surrounded cities. Thus, the only water exchange occurs through communication with the James River. However, waters typically fresher than the James River are found toward the head, indicating some other permanent input. The lower Nansemond River, where the data were collected, features a curved funnel shape, the transverse length of the subestuary decrease from ~4 to ~2 km between the entrance and the narrow channel (Fig. 1). The bathymetry consists of a channel flanked by shoals, but the position of the channel changes from the entrance to the head. The channel is located in the east side of the estuary entrance, and in the middle of the constriction, where also the deepest part of the channel is found (~6 m depth).

The James River estuary is the largest tributary in the lower Chesapeake Bay (Valle-Levinson et al., 2000). This estuary has received considerable attention over time (e.g., Pritchard, 1956; Moon and Dunstan, 1990; Friedrichs and Hamrich, 1996; Shen et al., 1999; Valle-Levinson et al., 2000). However, the small estuaries that discharge their waters into it remain unstudied. In the lower bay more than 80% of the variability exhibited by the currents is explained by the semidiurnal tides, where M_2 is the most important constituent, followed by N_2 , and S_2 (Browne and Fisher, 1988; Piñones, 2006). The interaction between M_2 and S_2 causes fortnightly variability generating differences in

the baroclinic pressure gradients, advective accelerations and friction between neap and spring tides (Valle-Levinson et al., 2000).

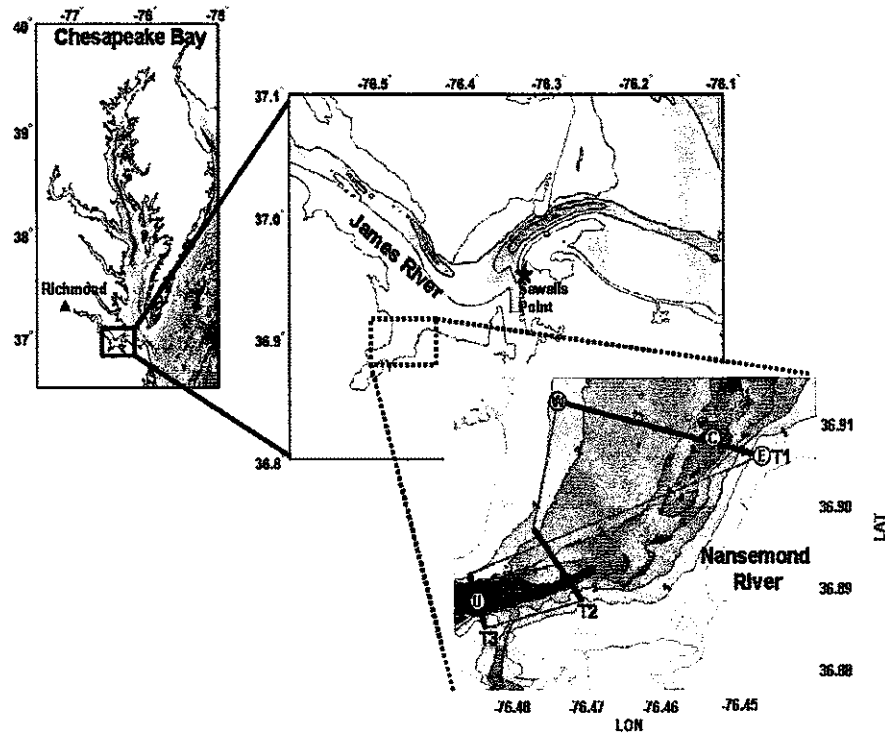


Fig. 1. Map of the study area at the Nansemond River estuary in the lower Chesapeake Bay. ADCP data were recorded along three cross-estuary transects (solid lines) referred to T1, T2 and T3 in the text. Along the complete track (solid and thin line) surface conductivity and temperature were also obtained. W, C and E correspond to CTD casts taken at the west, center and east side in T1. A fourth CTD cast was carried out at the center of T3 (U). Additionally two ADCPs were deployed over the shoals (W) and in the channel (C) during winter 2003-04 and summer 2004. River discharge data were recorded near Richmond, VA (solid triangle). Wind and sea level measurements were obtained from Sewells Point (solid star).

Specifically in the study area there are no studies that show wind variability. However at the entrance to Chesapeake Bay, winds have a strong seasonal signal, blowing from the northeast during late summer and early spring and from the southwest

during summer (Paraso and Valle-Levinson, 1996). The last 60 years of monthly river discharge for the James River, near Richmond, Virginia, show the highest values between February and April ($\sim 335 \text{ m}^3 \text{ s}^{-1}$) and the lowest between July and September, with an average of $\sim 95 \text{ m}^3 \text{ s}^{-1}$ (U.S. Geological Survey, Hydrologic Unit Code 02080205, <http://waterdata.usgs.gov/va/nwis/monthly>).

In the lower James River estuary, where the Nansemond river is located, subtidal outflows are well developed over the shoal and toward the left (looking into the estuary) and subtidal inflows in the channel toward the right as a result of Earth's rotation, advective accelerations and friction that balance the baroclinic pressure gradient (Valle-Levinson et al., 2000). Therefore, lighter waters are deflected to the left (looking into the estuary) and produce stronger cross-estuary density gradients ($0.7\text{-}2 \text{ kg m}^{-3} \text{ km}^{-1}$, Valle-Levinson et al., 2000) than along-estuary gradients ($0.2 \text{ to } 0.5 \text{ kg m}^{-3} \text{ km}^{-1}$, Hepworth and Kuo, 1989). Numerical models for the James River have shown numerous eddy formations (Shen et al., 1999; Shen et al., 2006). Their presence is the result of the interaction among tidal effects, local bathymetry and stratification (Shen et al., 1999). Further, these eddies have been considered to be responsible for larval retention in the lower James River estuary (Shen et al., 1999).

CHAPTER 3

DATA COLLECTION AND PROCESSING

Four oceanographic surveys were carried out in spring and fall of 2000 in order to record currents and hydrographic data during two spring tides (May 14-15, October 30-31) and two neap tides (May 22-23, October 20-21). Each survey consisted of repetitions of three cross-estuary transects during two semidiurnal periods (~25 hrs) using a towed, downward-pointing 1200 kHz acoustic Doppler current profiler (ADCP). The transects will be referred to as T1, T2 and T3 going from the entrance to the head of the subestuary and the four surveys will be designated as N1, N2, N3 and N4.

The ADCP was programmed to record velocity profiles each 2 seconds using a bin size of 0.5 m. To ensure the adequate temporal coverage, the three transects were sampled over a period of ~1.15 hours. This allowed the execution of an average of 15 repetitions per transect and permitted adequate isolation of tidal and subtidal effects on the current data (Valle-Levinson et al., 2000). A Seabird SBE37 conductivity-temperature (CT) sensor was attached to the towed ADCP to acquire surface temperature, salinity and density data along each transect. Also temperature, salinity and density profiles were sampled in each cruise using a Seabird 19 CTD. Three CTD casts were taken during each circuit repetition, at the river mouth transect at the west (W), center (C) and east (E) stations (Fig. 1). A fourth CTD (U) station was carried out in the middle of T3 (Fig. 1).

The ADCP data processing consisted of compass calibration and data correction following Joyce (1998). Further, current data were gridded onto uniform grids, which resulted in transects with horizontal resolution of approximately 20 m and vertical

resolution of 0.5 m. All the current velocity data were rotated along the maximum variance axis, which was close to the orientation of the main channel and the shore of the estuary. A least squares harmonic analysis for the two most important tidal constituents, semidiurnal (12.42 h) and diurnal (23.9 h) tides, was conducted for each grid node (e.g. Valle-Levinson et al., 1998) in order to get the amplitude and phase of these 2 constituents and the residual current (without tidal effects) for each grid point. In general, the differences between the fit and the data sampling were less than 0.1 m s^{-1} and the variability explained by the fit was more than 85%, which indicated that the fit captured well the real variations of tidal currents. Since the CTD and CT records were nearly equally distributed along the different tidal phases a simple average seems to be an appropriate representation of the residual field of the hydrographic variables during each cruise.

In order to describe the subtidal variability of the exchange between the estuary and the subestuary, ADCPs were deployed in the channel and over the shoals at the entrance to the Nansemond River. The data were recorded during two periods, between November 17, 2003 and February 8, 2004 (hereafter, referred to as winter deployment) and between April 29 and July 22, 2004 (hereafter, referred to as summer deployment). For each deployment a 600 kHz ADCP was bottom-mounted in the channel (~ 4 m) and a 1200 kHz ADCP over the shoals (~ 2 m) (similar to the locations of CTD, "C" and "W" in Fig. 1). The ADCP over the shoals during the summer deployment recorded valid data between April 29 and June 8. Each ADCP was set to record a velocity profile every 15 m using a bin size of 0.5 m. During the winter deployment conductivity and temperature data in the channel were recorded in addition to current data using a bottom-mounted CT

at intervals of 15 m. All the ADCP were also equipped with built in bottom pressure sensor recording data every 15 m.

Hourly time series of wind speed and direction corresponding to all collected data were obtained from Sewells Point (station # 8638610) at Norfolk, VA (Fig. 1). This station is maintained by NOAA's National Ocean Service and the data are available from the Center for Operational Oceanographic Products and Service (<http://www.co-ops.nos.noaa.gov/>). Also, daily river discharge was obtained from the U.S. Geological Survey for the James River near Richmond, VA (Hydrologic Unit Code 02080205, <http://waterdata.usgs.gov>). Data from ADCPs and CTs were averaged hourly in order to make them comparable with wind data. River discharge was hourly interpolated with the same objective. Since the aim of this work was to study the subtidal exchange, all the time series were filtered using a low-pass filter of half power of 30 hrs. The filtered current data over the shoals and in the channel were rotated along the axis of the main channel at the entrance of the Nansemond River (~15° clockwise). Therefore, hereafter the flow components will be referred to as along-channel and cross-channel flow. The filtered wind data was rotated along the main axis of the James River estuary at Sewells Point (~47° clockwise), therefore hereafter wind components will be referred to as along-estuary and cross-estuary wind.

The relationships among the measured variables were analyzed using different time series techniques according to Emery and Thompson (1998). Cross correlation analyses were performed among winds, sea level and currents at depth. Spectral analysis and coherence together with phase spectra were performed using 8 degrees of freedom and ~2000 data points (n) for each deployment using Welch's methods. Empirical

orthogonal functions (EOF) were derived for the subtidal moored current data in order to find the dominant modes of variability. The EOFs were calculated following the standard procedure suggested by Emery and Thompson (1998), using the along-channel filtered rotated flow for all depths in the channel and over the shoals. Therefore the EOFs were composed of 5 variables for the channel and 5 variables for the shoals. The different modes of variability were compared with the along-estuary wind and the shear velocity as a representation of estuarine circulation.

CHAPTER 4

RESULTS

The results are presented as follows: first, the current data recorded during the four surveys were analyzed in terms of the main features identified during each survey. These features were determined by wind, river discharge, salinity fields and volume fluxes. Afterward, these results were extended through the analysis of time series for the winter and summer deployments.

4.1 Oceanographic surveys

4.1.1 Atmospheric and hydrographic conditions

Winds were variable during the cruises without a clear predominance (Fig. 2a, b). While northward winds occurred during N1 and N4 with speeds between 2 - 3 m s⁻¹, northwestward and northeastward winds were recorded during N2 and N3, respectively. Wind speeds were slightly higher at N3 (~5 m s⁻¹) than at N2 (~3 m s⁻¹). The James River discharge showed the typical seasonal pattern, i.e., greater discharges in spring (May surveys) than fall (Oct-Nov surveys) (Fig. 2c, d). In general the river discharge was < 250 m³ s⁻¹ in N1, N3 and N4. However, N2 was carried out under the highest river discharge of all the surveys (~800 m³ s⁻¹). The effects of these differences in discharge over the subestuary were clearly observed in the distributions of salinity (Fig. 3). During low discharge (N1, N3 and N4) the horizontal salinity fields at surface showed a weak along estuary gradient (<1 psu). High salinity appeared at the entrance of the Nansemond River and decreased toward the head of the subestuary (Fig. 3a, e, g). However, during high river discharge (N2) the lowest salinity of the four cruises occurred as fresh water

intruding through the northwest (8-9 psu) causing appreciable transverse gradients even at the constriction of the subestuary (Fig. 3c). These surface features were also well represented in the vertical profiles (Fig. 3b, d, f, h) suggesting that the intrusion from the estuary (James River) affects the salinity distribution and therefore changes the sign of the baroclinic pressure gradients of the subestuary, at least in the area studied. At the entrance to the subestuary the stratification was slightly stronger (top-to-bottom $\nabla\rho \approx 0.3 \text{ kg m}^{-3}$) than up the subestuary ($\nabla\rho \approx 0.08 \text{ kg m}^{-3}$). This probably resulted from the major influence of the James River and the depth of the water column. However, the vertical changes in salinity were no greater than 0.5 – 1 psu. Thus the Nansemond River can be considered a partially mixed estuary, similar to James River (Valle-Levinson et al, 2000).

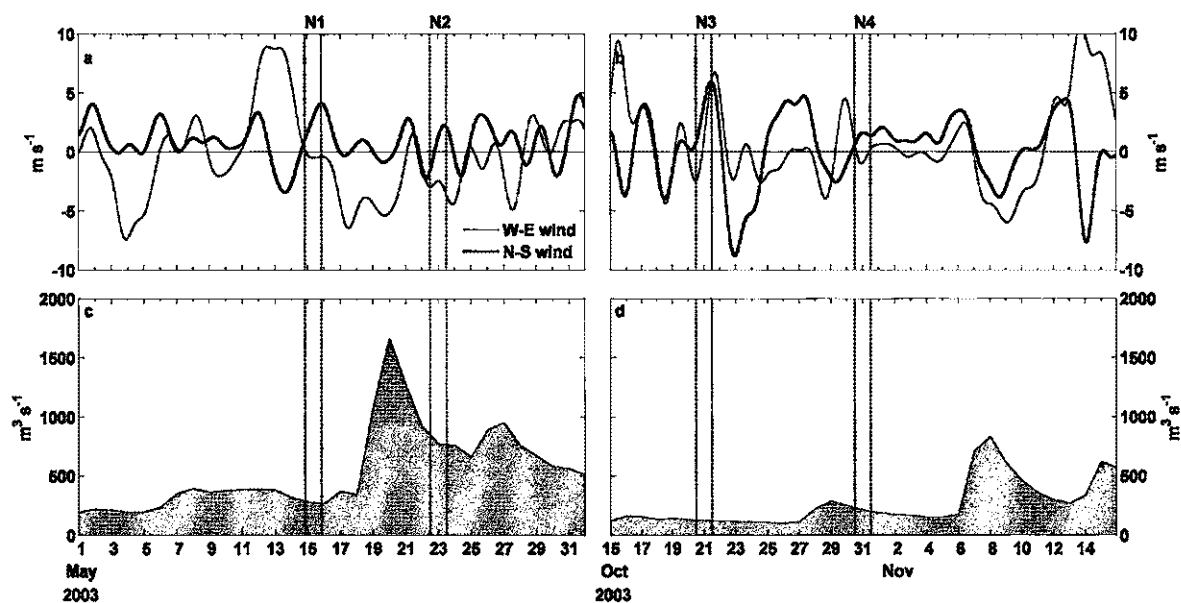


Fig. 2. Time series of wind (a-b) and river discharge (c-d) for each survey. W-E and N-S wind components are in oceanographic convention, positive values represent eastward and northward winds respectively. Vertical dashed lines correspond to the date when each survey was carried out.

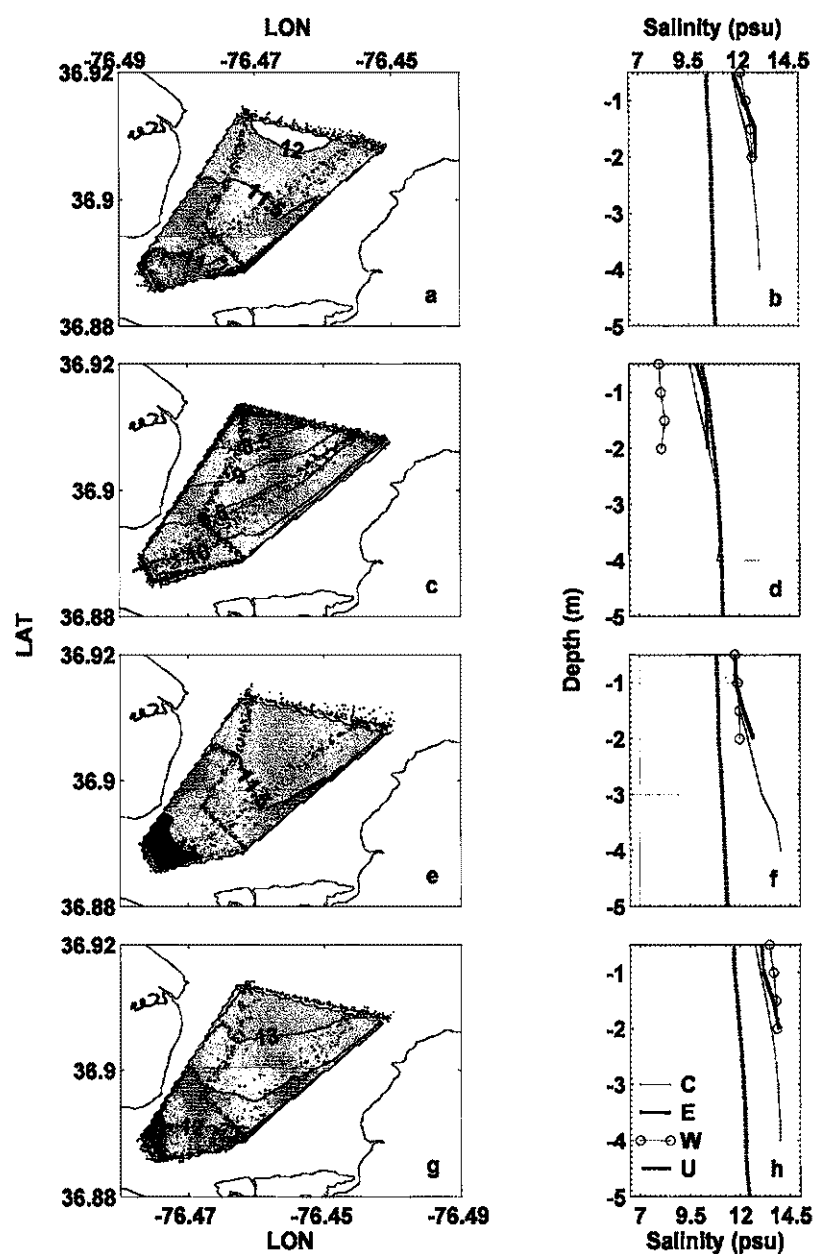


Fig. 3. Mean horizontal surface salinity fields and mean salinity profiles during N1 (a,b), N2 (c,d), N3 (e,f), and N4 (g,h). W, C, E and U are the CTD cast at the west, center, east and up-subestuary, respectively. Dotted line represents the CT's path.

4.1.2 Subtidal circulation

Subtidal current fields also showed differences among surveys (Fig. 4). At T1 a well-developed estuarine circulation occurred in the channel, i.e., surface outflows and

sub-surface inflows. Over the shoals, the water column is ~1 m deep and unidirectional flow through this shallow water column was observed (Fig. 4a).

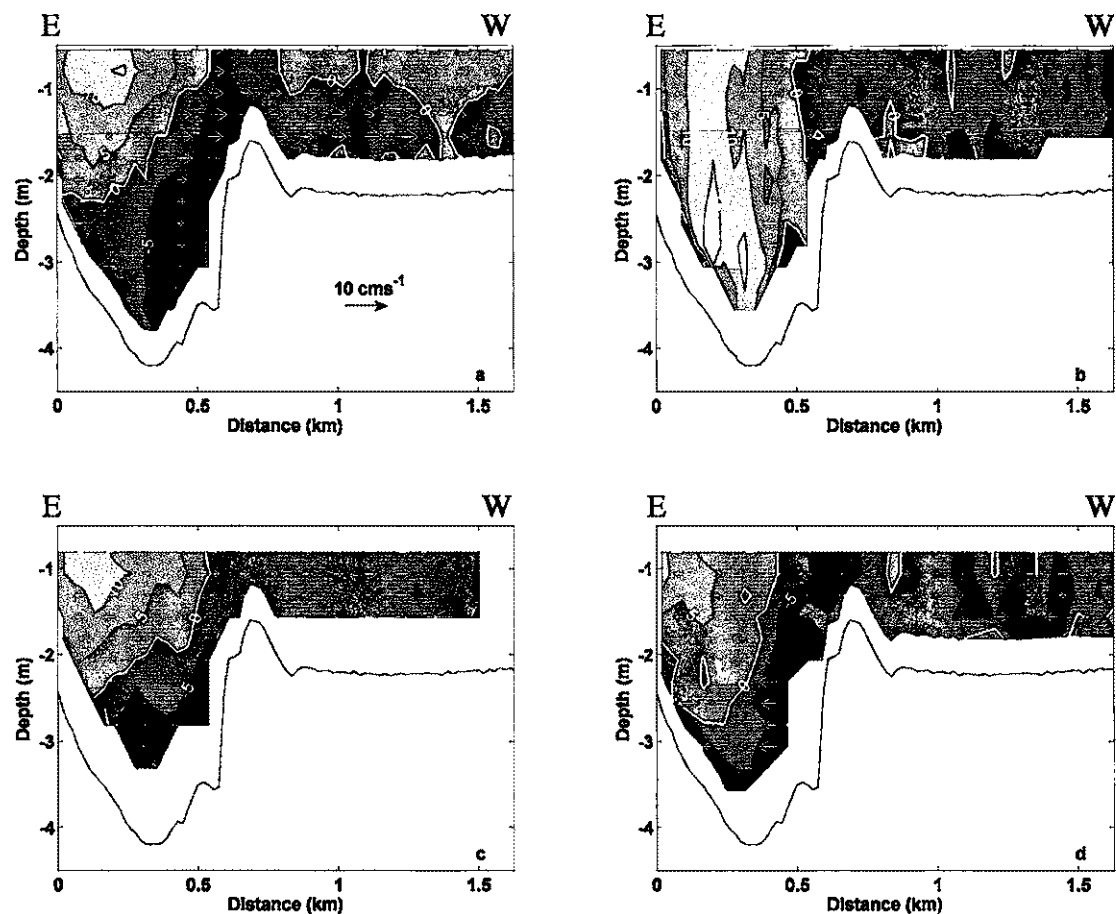


Fig. 4. Subtidal flow at T1 during N1 (a), N2 (b), N3 (c) and N4 (d). Gray colored contours represent the along-channel flow and white arrows the cross-channel flow. Light gray corresponds to outflows (looking into the estuary) and E, W refer to the east and west side of the subestuary respectively. The white line indicates zero velocity.

The flow followed the orientation of the main channel of the subestuary. Hereafter, the components of the flow will be referred to as along-channel and cross-channel. Although the flow was mostly along-channel, significant lateral circulation or

cross-channel flow occurred mainly over the shoals. Westward currents were predominant over this area close to the right shore (looking into the estuary) and eastward currents close to the left shore. During the survey when the change in the direction of the pressure gradient occurred, i.e., N2, the near-bottom inflow that appeared in the channel during the other surveys was reversed. As a result, unidirectional outflow appeared in the entire channel (Fig. 4b). However, over the shoals the circulation remained similar to the other surveys. The transverse partition observed at T1 was less evident further upstream into the subestuary (Fig. 5).

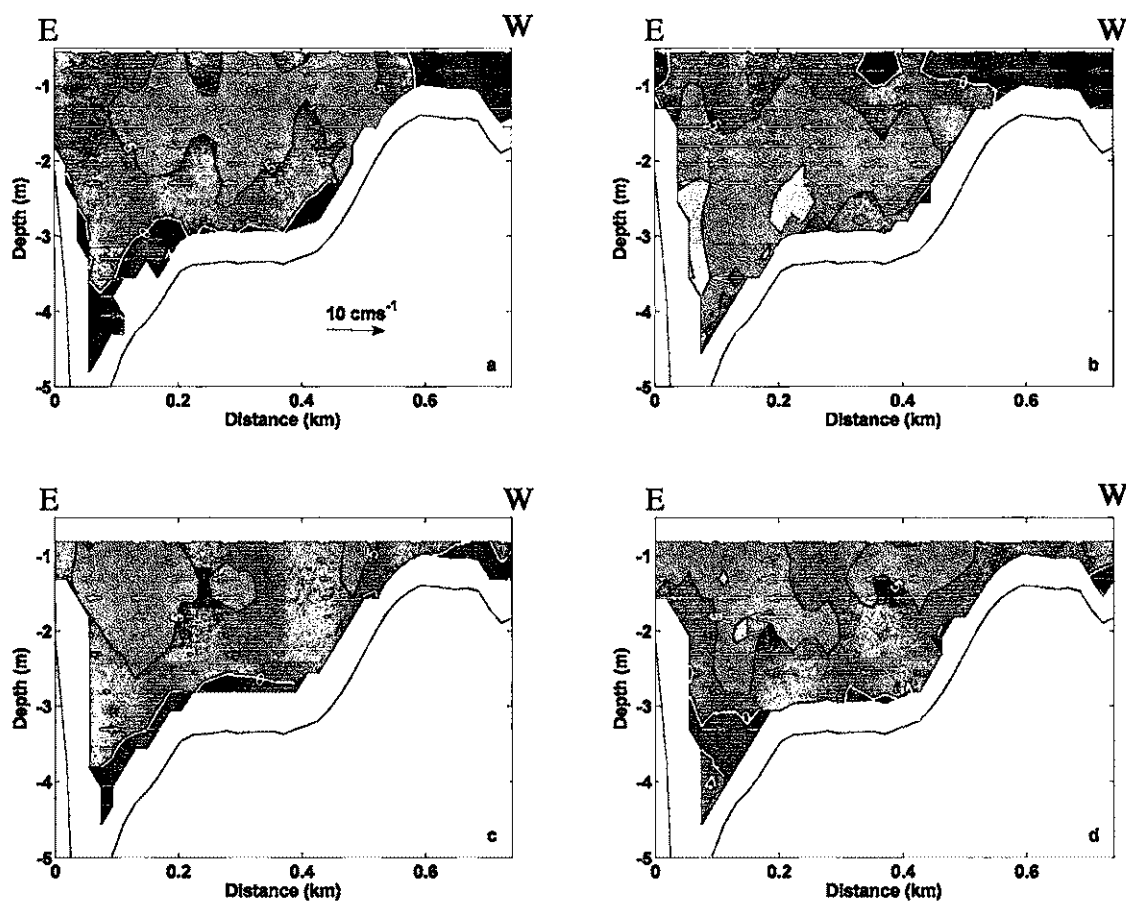


Fig. 5. Same as Fig. 4 but for subtidal flow at T2.

At T2 outflows appeared over most of the transect and inflows only occurred near the bottom in all the surveys and over the shoals in N1 and N2 (Fig. 5a, b). Strong cross-channel circulation was observed only during N2 (Fig. 5b), which might have been caused by the intrusion of freshwater. For T3 the currents also showed large transverse variability despite the short length of this transect (Fig. 6a, b, d). Outflow occurred throughout the entire water column at the right side (looking into the estuary) and inflow appeared in the left side mainly during N1, N2 and less evident in N4. During N3 inflow was observed in the entire transect (Fig. 6c).

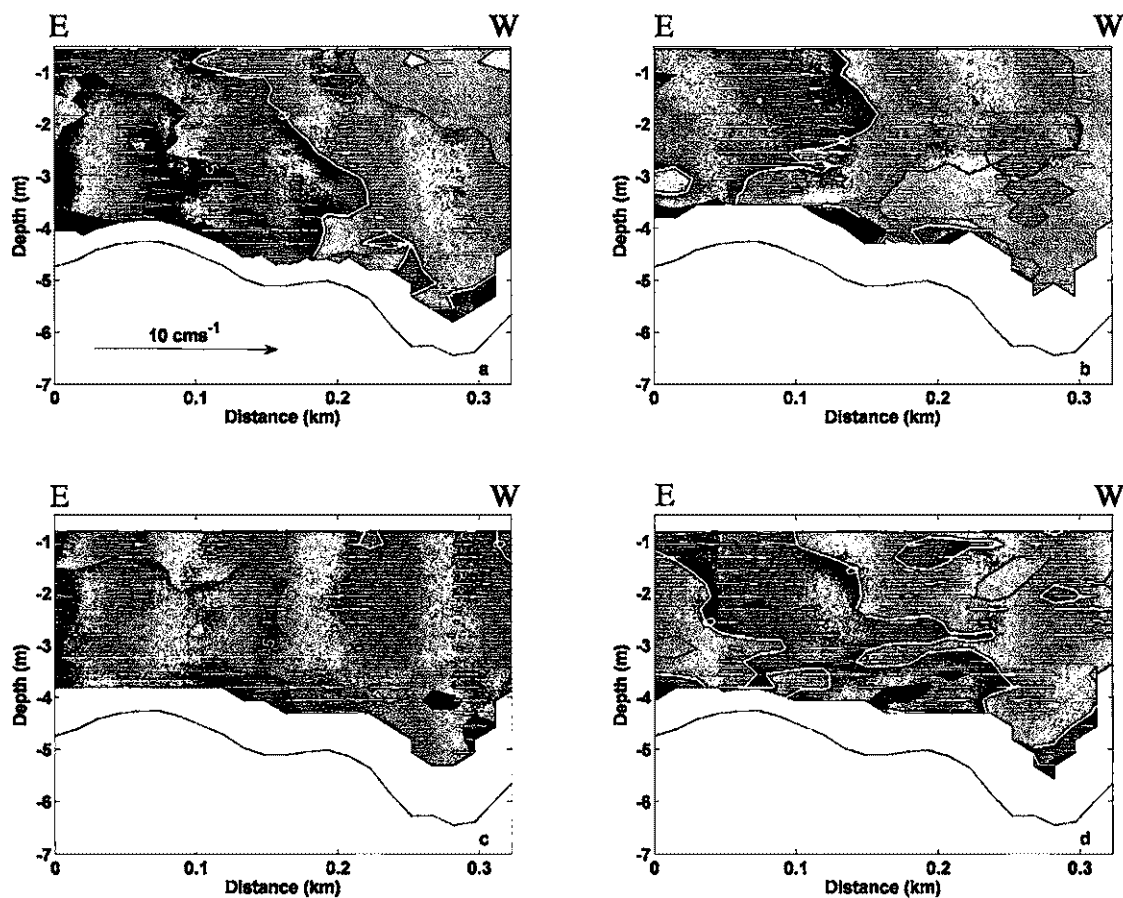


Fig. 6. Same as Fig. 4 but for subtidal flow at T3.

A comparison among transects of the mean velocity profile in the channel (Fig. 7) confirmed these facts and revealed other important features in the circulation.

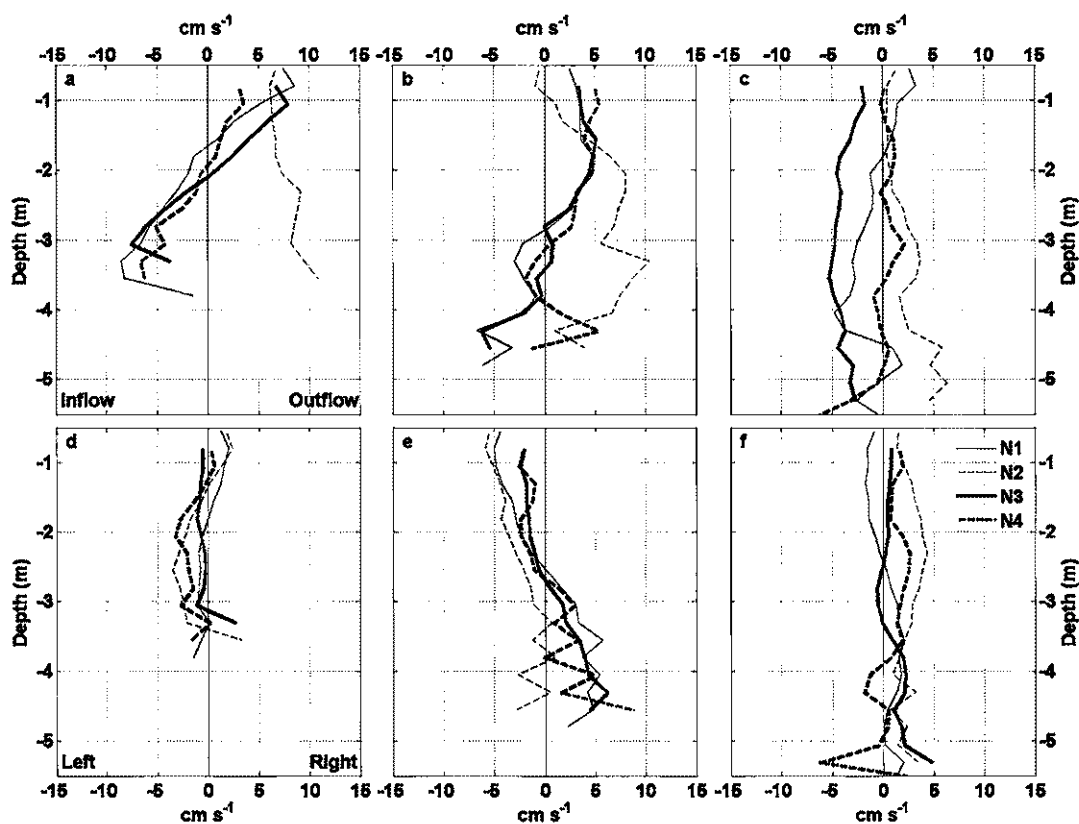


Fig. 7. Mean velocity profile for each survey in the channel at T1 (a,d), T2 (b,e) and T3 (c,f). Upper panels correspond to the along-channel flow (a-c) and bottom panels correspond to the cross-channel flow (d-f).

At T1 (Fig. 7a) along-channel outflows and inflows were well separated and the change between inflows and outflows appeared at ~ 2 m. The depth-independent outflow during N2 at T1 appeared in the mean (Fig. 7). For the cross-channel currents, the flow in the first 2 m tended to be rightward (looking into the estuary) but leftward underneath.

However, the magnitudes of the currents were weaker than along-channel flows (Fig. 7d). At T2 (Fig. 7b) surface outflows (1–3 m) and sub-surface inflows (3–5 m) also occurred although they were not as obvious as in T1. Transect N2 showed differences: the lateral circulation in this transect was better developed than in the others with leftward surface flows (1–3 m) and rightward flows under 3 m (Fig. 7e). At T3 weaker and depth-independent flows were observed in both along and cross-channel flows (Fig. 7c, f).

The horizontal velocity fields at the surface not only confirmed previous results, but also showed circulation patterns that suggested a recirculation area at the entrance of the subestuary (Fig. 8).

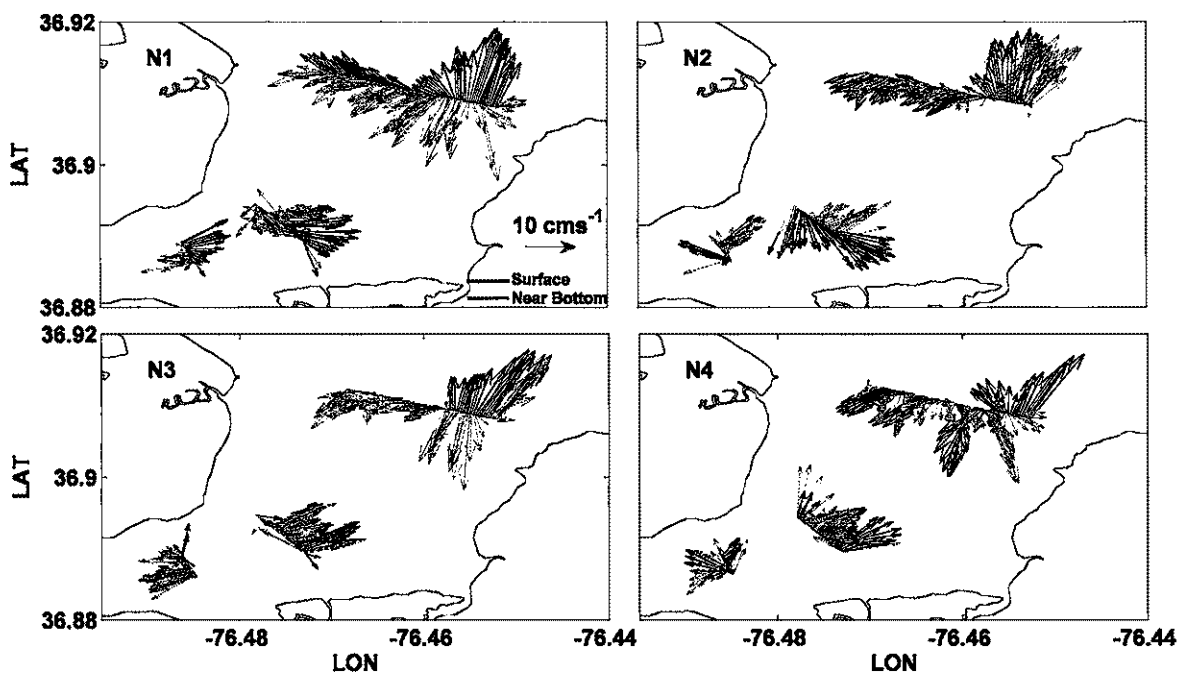


Fig. 8. Horizontal currents field for N1, N2, N3 and N4 (a, b, c, d, respectively). Dark arrows indicate the surface flow (~1.5 m below the surface), and light arrows represents the near bottom flow (~1.5 m upper the bottom).

During N1 (Fig. 8a), this recirculation was less evident than during the other cruises. However for N2 (Fig. 8b), the recirculation was most obvious, as shown by the lateral southeastward flow at T2 and westward currents over the shoals at T1. During N3 (Fig. 8c) and N4 (Fig. 8d) inflow (westward and southwestward flow) was observed over the shoals at T1, but at T2 all the flow was outward (northeastward), suggesting that at some point between T1 and T2 there was a recirculation of the flow. This recirculation is evaluated quantitatively with volume fluxes (next section).

4.1.3 Volume flux estimations

Because of conservation of volume, the inflow and outflow Q (in $\text{m}^3 \text{s}^{-1}$), through the transects should be equal, i.e., Q through T1 \approx Q through T2 \approx Q through T3. To estimate volume fluxes, we used the relation $Q = V \times A$, where V is the mean inflow or outflow (in m s^{-1}) and A is the area of the respective transects (in m^2). An estimation of inflow/outflow volume flux for each transect was thus obtained. The results, however, did not show conservation of volume (Table 1). Overall, the outflow volume flux (Q_{out}) decreased monotonically between T1 and T3 except for N4 where an increase occurred. The greatest difference in Q_{out} occurred between T2 and T3. For instance, during N1 and N3, Q_{out} was very similar between T1 and T2, but decreased more than 50% between T2 and T3. The inflow volume flux (Q_{in}) showed a different pattern: decreases occurred between T1 and T2 with differences of more than 60%, while between T2 and T3 there were increases instead of decreases as observed for Q_{out} . These results confirm the idea of a return of the flow between T1 and T2. Q_{in} in T1 is several times greater than Q_{in} in T2,

suggesting an apparent loss in volume. On the other hand, Q_{out} increases from T2 to T1, indicating an apparent gain in volume between T1 and T2.

Table 1

Estimations of mean volume fluxes separated by survey and transects. Inflow (Q_{in}) and outflow (Q_{out}), Q units are in $m^3 s^{-1}$

Transect	N1		N2		N3		N4	
	Q_{in}	Q_{out}	Q_{in}	Q_{out}	Q_{in}	Q_{out}	Q_{in}	Q_{out}
1	80.8	57.4	49.8	125.5	67.5	66.3	105.5	35.0
2	16.1	55.0	14.6	78.4	6.2	60.0	6.7	68.2
3	39.9	26.9	15.7	38.2	58.9	1.0	15.3	20.8

The previous estimates did not consider changes in the area of each transect, which varied from ebb to flood tides owing to sea level changes. Furthermore, the shallow water near the shore (< 1m) was inaccessible by boat. Thus a rough estimation indicates that the transverse area measured in this study was between 50 and 75% of the total transverse area of the subestuary. In consequence, it is possible that the lack in volume flux noted above can be compensated for the area not covered in our measurements. In order to evaluate this possibility, the volume flux at the unmeasured area that satisfied the condition of volume conservation (Table 2) was calculated by subtracting the inflow/outflow volume flux between the transects, i.e., $Q_{est} = Q_{T1} - Q_{T2}$; $Q_{est} = Q_{T2} - Q_{T3}$. The unmeasured area (A_u) was calculated as the difference between the total area (A_t) and the measured area (A_m). A_t was obtained considering an average of A_m and extrapolating to the shore. The variations of area owing to changes in sea level were not taken into account. Knowing Q_{est} and A_u it was possible to estimate the flow speed (V_{est}) through A_u that satisfies volume conservation. Then, V_{est} was compared against

mean speed observed (V_{obs}) at the transect where the reduction or increase in the volume flux occurred.

Table 2

Volume fluxes (Q_{est}) and velocity estimations (V_{est}) for outflows and inflows through the area not covered during the data collection. Q_{obs} and V_{obs} are the volume flux and velocity observed. Q units are in $m^3 s^{-1}$, V are in $m s^{-1}$. See text for data interpretation

Cruise	Comparison	Transect	Outflow			
			Q_{obs}	V_{obs}	Q_{est}	V_{est}
N1	T1-T2	2	55.0	0.045	2.4	0.003
N2			78.4	0.058	47.1	0.063
N3			60.0	0.040	6.3	0.008
N4		1	35.0	0.035	-33.2	0.032
N1	T2-T3	3	26.9	0.038	28.0	0.035
N2			38.2	0.040	40.1	0.050
N3			1.0	0.019	59.1	0.074
N4			20.8	0.025	47.5	0.059
			Inflow			
			Q_{obs}	V_{obs}	Q_{est}	V_{est}
N1	T1-T2	2	-16.1	-0.032	64.7	0.086
N2			-14.6	-0.038	35.2	0.047
N3			-6.2	-0.026	61.2	0.081
N4			-6.7	-0.031	98.8	0.131
N1	T2-T3	2	-16.1	-0.032	-23.7	-0.030
N2			-14.6	-0.038	-1.1	-0.001
N3			-6.2	-0.026	-52.7	-0.066
N4			-6.7	-0.031	-8.6	-0.011

There were three possible cases: (1) the inflow/outflow speeds at the sides were slower than the speed measured; (2) similar speeds, meaning a constant inflow/outflow speed from side to side of the estuary and (3) the speed at the sides was faster than the speed measured. The first case was indeed the most probable or realistic as bottom and lateral friction play an important role in decreasing the flow speed at the bottom and close to shore. The second case was less probable but under strong flow it might be possible.

However it is physically impossible for the third to have occurred because of the effects of lateral and bottom friction on the flow. Accordingly, only the first two situations were considered. Thus if $V_{est} \leq V_{obs}$ the deficit in the inflow/outflow volume flux could be explained as flow going through the unmeasured area. The results are presented in Table 2. For instance, the outflow volume flux through T1 at N1 ($Q_{out-T1-N1}$) was $57.4 \text{ m}^3\text{s}^{-1}$ and $Q_{out-T2-N1} = 55 \text{ m}^3\text{s}^{-1}$ (see Table 1). The difference between the transects was $2.4 \text{ m}^3\text{s}^{-1}$ (Q_{est} , for the outflow at N1, comparison T1-T2 at Table 2). That means there was a gain of $2.4 \text{ m}^3 \text{ s}^{-1}$ in T1 ($Q_{out-T1-N1} > Q_{out-T2-N1}$), so that the speed needed through the unmeasured area at T2 should be 0.003 m s^{-1} (V_{est} at Table 2). This speed is much smaller than the outflow speed through T2 ($V_{obs} = 0.045 \text{ m s}^{-1}$), suggesting that it is possible that the gain in Q at T1 may be compensated by flow in the unmeasured area. In general it can be seen that, for the outflow, the estimated speed was lower or similar to the observed speed, the exception being the third and fourth cruises between T2 and T3 where $V_{est} > V_{obs}$. The inflow results showed disparities: most values of V_{est} were much greater than those of V_{obs} , mainly between T1 and T2, suggesting that the flow close to the edges of the subestuary is greater than the flow in the middle of the subestuary, i.e., the third case mentioned above, which was unlikely. Therefore, this result a) suggests that a compensatory volume flux should not occur through the unmeasured area, and b) reinforces the idea of a return flow or a recirculation zone.

Although the volume flux estimations and the results of the data recorded during the surveys provided some insight into the subtidal circulation in the Nansemond River, the temporal resolution was not good enough to explain the variations observed. Hence several questions remain unanswered. Some of these are: Is the recirculation area a

permanent feature of the Nansemond River? Is the unidirectional outflow observed in the channel a consequence of the recirculation area? How does wind affect this circulation pattern? In order to describe the temporal variability of the subtidal flow, an analysis of moored ADCP, wind stress, sea level and river discharge data during a winter and summer deployment is presented in the next section.

4.2 Temporal variability

To explore the temporal variability of the subtidal flow, the low-pass filtered records were first analyzed in the time domain and the relationship among them through correlation analysis was explored afterward. Next, to find the predominant temporal scale in the data, frequency domain analysis was performed using Fourier analysis as well as coherence and phase spectra. Finally, the most important modes of variability in the circulation as well as the forcing of these modes were investigated with Empirical Orthogonal Functions.

4.2.1 Time domain analysis

During winter, currents were in opposite direction in the channel than over the shoals, i.e., when inflow was observed over the shoal outflow appeared in the channel and vice-versa (Fig. 9a, b). However, during certain periods, outflow was observed over the shoals and channel simultaneously (e.g. Dec 15, Jan 1). The typical estuarine circulation (surface outflow and sub-surface inflow) observed in the surveys (see Fig. 4, N1, N3 and N4) was not prevalent during the winter deployment. Instead, unidirectional

flows in the channel and over the shoal were more common during most of the time (Fig. 9a, b).

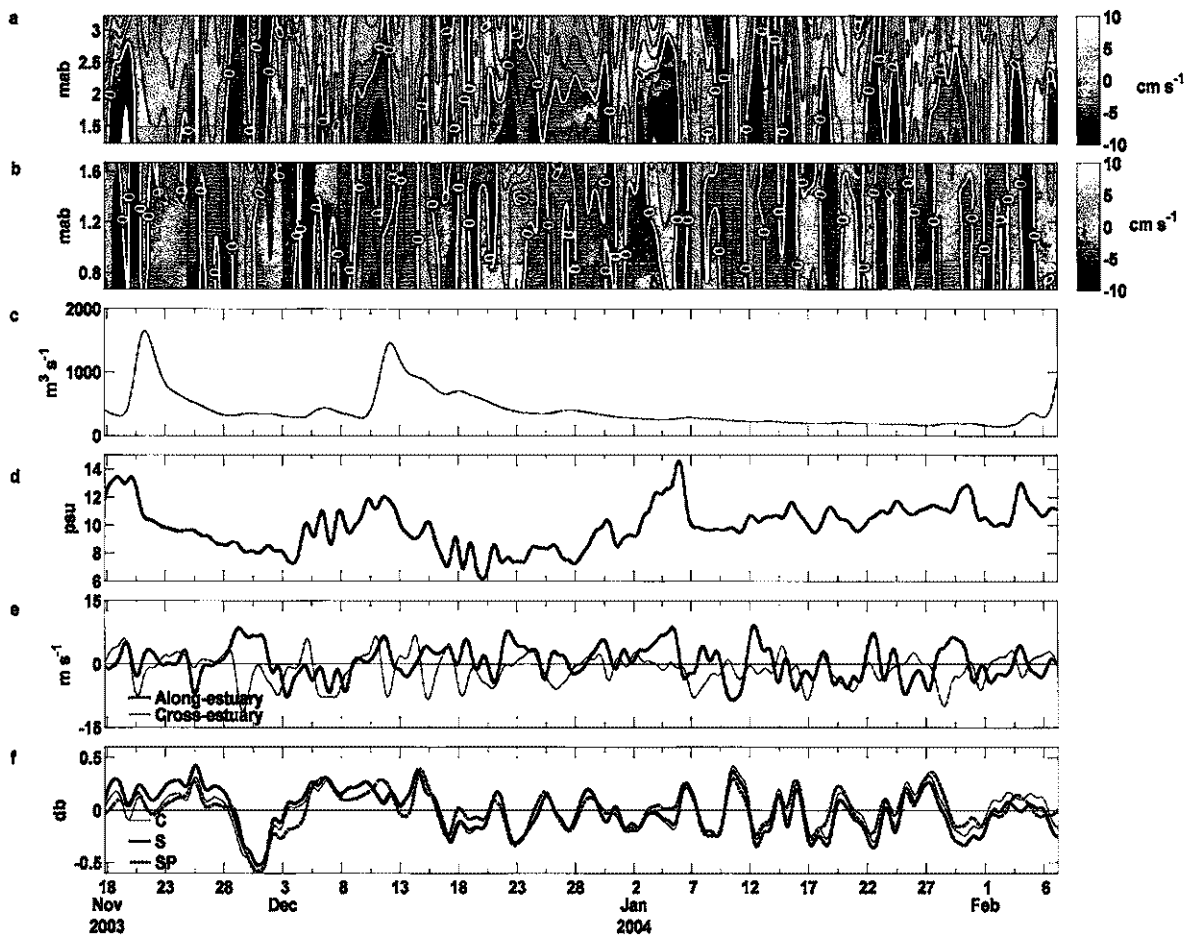


Fig. 9. Time series for the winter deployment. Along-channel currents (a) in the channel, (b) over the shoals, (c) James River discharge, (d) bottom salinity in the channel, (e) wind components, and (f) bottom pressure in the channel (C), over the shoals (S) and sea level at Sewells Point (SP). Winds and currents are in oceanographic convention. The ordinate in the current contours (a and b) shows meters above the bottom (mab)

A few pulses of river discharge occurred in early winter (Nov 19-22; Dec 10-15) followed by periods of weak variability (Fig. 9c). The temporal pattern in salinity differed from that in river discharge, showing more variability than the two drops related

to the river (Fig. 9d). Because of the distance between the river discharge and salinity gauges, a time lag between the series could be expected. In fact, the minimum salinity occurred ~7-9 days after the maximum in river discharge ($r = -0.6$, $p < 0.05$). However, this correlation might be explained only by the two large drops in salinity that occurred on Dec. 4 and 20 after the increase in the river discharge on Nov 22 and Dec 12, respectively. On the other hand, the correlation between river discharge and along-channel flow was not significant. Therefore, besides the good relationship observed during N2 among the increase in the river discharge, the decrease of salinity and the unidirectional outflow in the channel, in a longer period of time, the relationships are not clearly established.

The principal axis of the wind during this season was ~40° clockwise, i.e., similar to the main axis orientation of the James River estuary at Sewells Point (~47° clockwise). Therefore rotated wind components contained both the maximum variance axis (along-estuary wind) and the minimum variance axis (cross-estuary wind). Positive values of along-estuary wind and cross-estuary wind correspond to northeastward wind (wind blowing outward the estuary) and northwestward wind, respectively. Outward and inward wind pulses were predominant during this deployment with the along-estuary wind component greater in magnitude than the cross-estuary wind component (Fig. 9e, Table 3). Along-channel currents showed significant correlation at all depths with the along-channel wind, with a maximum ($r = -0.6$, $p < 0.05$) at 2.6 mab (meters above the bottom) in the channel. Over the shoal significant values of correlations were observed ($r > 0.4$, $p < 0.05$) with a maximum ($r = 0.6$, $p < 0.05$) between 0.8 and 1.4 mab. Note that in this case the series had a positive correlation.

Table 3

Wind statistics for winter and summer deployments, units are in m s^{-1}

	Winter		Summer	
	Along	Cross	Along	Cross
Mean	0.5	-1.3	-1.8	-0.5
Std	3.4	3.1	2.3	1.9
Maximum	8.2	5.6	6.1	5.2
Minimum	-9.0	-9.5	-4.7	-5.1
Principal axis	40.3		71.2	
U %	49.2		62.2	
V %	50.7		37.8	

Sea level and bottom pressure showed a similar pattern of variability at the entrance to the Nansemond (C,S in Fig. 9f) and James River (SP in Fig. 9f). Because of the similar interpretation, hereafter bottom pressure will also be referred to as sea level. Increases and decreases in the sea level were regular in time except during the first month of measurements, when sea level dropped over a 5-day period (Nov 28 - Dec 3). Current and sea level were also well correlated at all depths with positive maximum ($r = 0.6$, $p < 0.05$) at the surface over the shoal and negative maximum ($r > -0.6$, $p < 0.05$) at 1.2 mab in the channel. Similarly, sea level was well correlated with wind as overall increases/decreases in sea level occurred during inward/outward wind (Fig. 9e, f). As a result along-estuary wind was negatively correlated to sea level ($r = -0.6$, $p < 0.05$), and cross-estuary wind showed correlations just of -0.3 , slightly above the significance level.

Similar to the winter deployment, unidirectional and bidirectional flows during the summer were the main feature of along-estuary flows in the channel (Fig. 10a). Again, unidirectional flow was present over the shoals, however opposite directions from channel to shoal flows was not clearly observed in this deployment (Fig. 10b). River

discharge was lower during summer than winter and showed more fluctuations (Fig. 10c) but it was not possible to determine the influence of the James River discharge on the Nansemond River salinity because no salinity information was available for this period. Nevertheless, similar results as in winter might be expected in view of the low discharge and weak correlation between river discharge and along-channel flow.

Wind also showed predominant outward and inward pulses. However, wind intensity was greater during this season than in winter and with lower variability (Fig. 10c, Table 3).

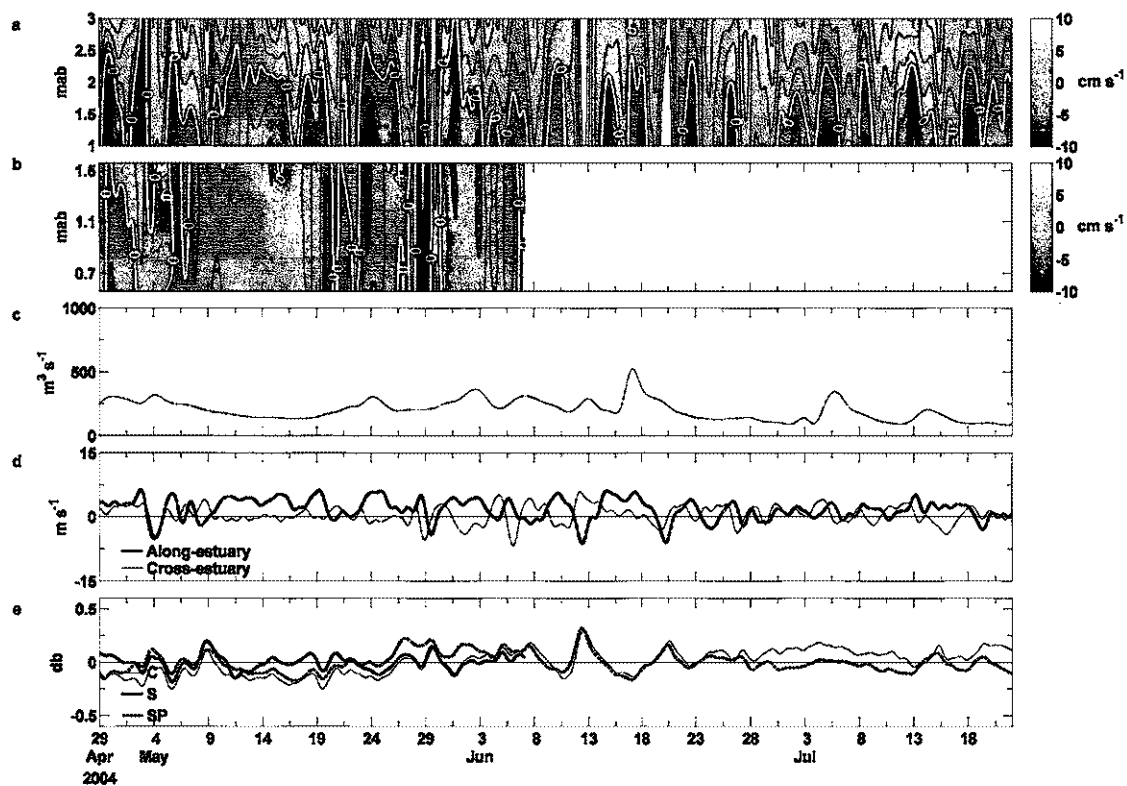


Fig. 10. Time series for the summer deployment. Along-estuary currents (a) in the channel, (b) over the shoals, (c) James River discharge, (d) wind components, and (e) bottom pressure in the channel (C), over the shoals (S) and sea level at Sewells Point (SP). Winds and currents are in oceanographic convention. The ordinate in the currents contours (a and b) shows meters above the bottom (mab)

During summer the principal axis of the wind was $\sim 70^\circ$ clockwise, i.e., differing by $\sim 30^\circ$ with the orientation of the main axis of the James River. Similar to winter, along-estuary wind showed negative correlation with along-channel flow over the entire water column in the channel ($r = 0.5$, $p < 0.05$). Similar but negative correlation values were obtained over the shoal, i.e., contrary to previous results. However this difference might not be reliable because of the shortness of the shoal current record. Cross-estuary wind showed significant negative correlation values only in the channel ($r = -0.4$, $p < 0.05$). Sea level variability was also lower and although the entire series (i.e., C, S, SP) showed similar fluctuations, they were not as well correlated as in the winter deployment (Fig. 10e). Along-estuary wind was only slightly correlated to sea level ($r = -0.3$, $p < 0.05$), while cross-estuary wind was better correlated to the sea level ($r = -0.5$, $p < 0.05$). The correlation analysis suggests that inward wind induces a depth-independent inflow over the shoal and a depth-independent outflow in the channel. This is equivalent to downwind currents over the shoals and upwind flows in the channel. The dominant temporal scales of the variability in the currents, wind and sea level are examined in the next section.

4.2.2 Frequency domain analysis

Although river discharge during winter showed low variability, a significant increase in the energy appears in the spectra around 0.1 cpd (~ 10 days) (Fig. 11a). However, it seems to be influenced by the two large increases previously described in the records rather than by a permanent cycle (see Fig.9c). Salinity also showed an energy increase at the same frequency (0.1 cpd) and at ~ 0.36 cpd (Fig. 11b) but the spectral

density was almost 4 times lower than that of river discharge. As a result no significant coherences were found between salinity and river discharge (Fig. 11c), supporting the correlations results presented above.

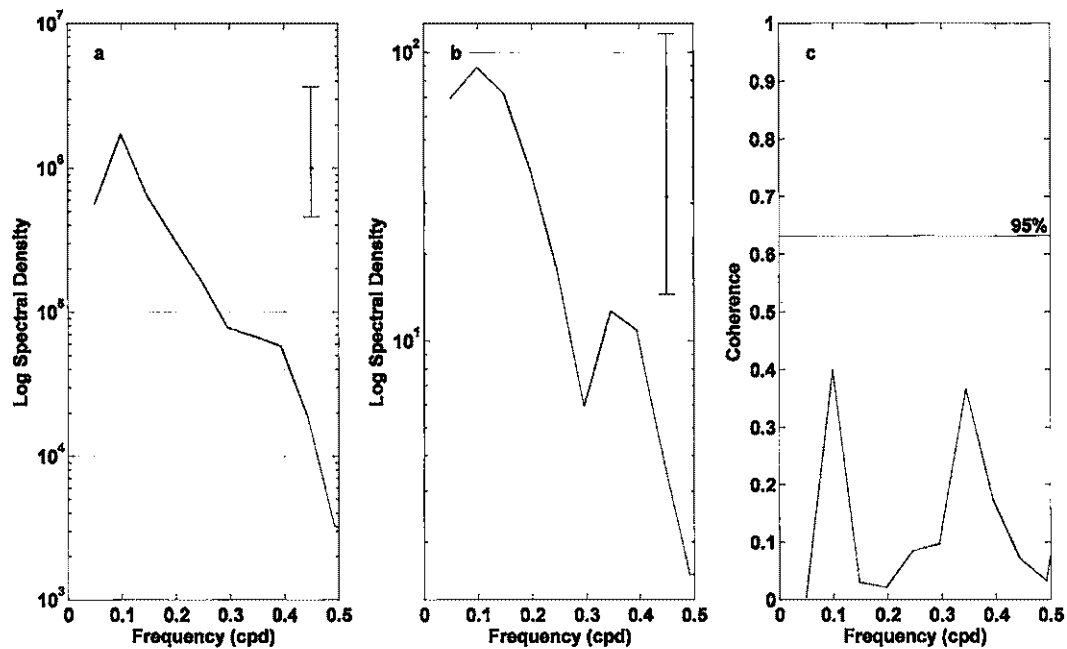


Fig. 11. Spectral analysis for James River discharge and bottom salinity in the subestuary for the winter deployment. (a) James River discharge spectra, and (b) bottom salinity spectra. (c) Coherence spectra between river discharge and salinity. Vertical line in (a) and (b) and horizontal line in (c) represents the 95% significance level.

The spectra for the different deployments in Figures 12 and 13 showed that synoptic scale (3-7 days) variability was predominant in most of the records. Over the shoals, spectral density of currents showed two peaks at 0.33 cpd (~ 3 days) and 0.14 cpd (~ 7 days) clearly distinguished at all depths (Fig. 12a). In the channels only the peak around 7 days was observed and not the one around 3 days with spectral densities more energetic than those observed over the shoals (Fig. 12b). The spectral density of the

along-estuary wind was slightly higher than that of the cross-estuary wind in the higher frequencies but not in the lower frequencies (>0.35 cpd). The dominant peak occurred at ~ 7 days (Fig. 12c), which was observed also for the sea level records (Fig. 12d).

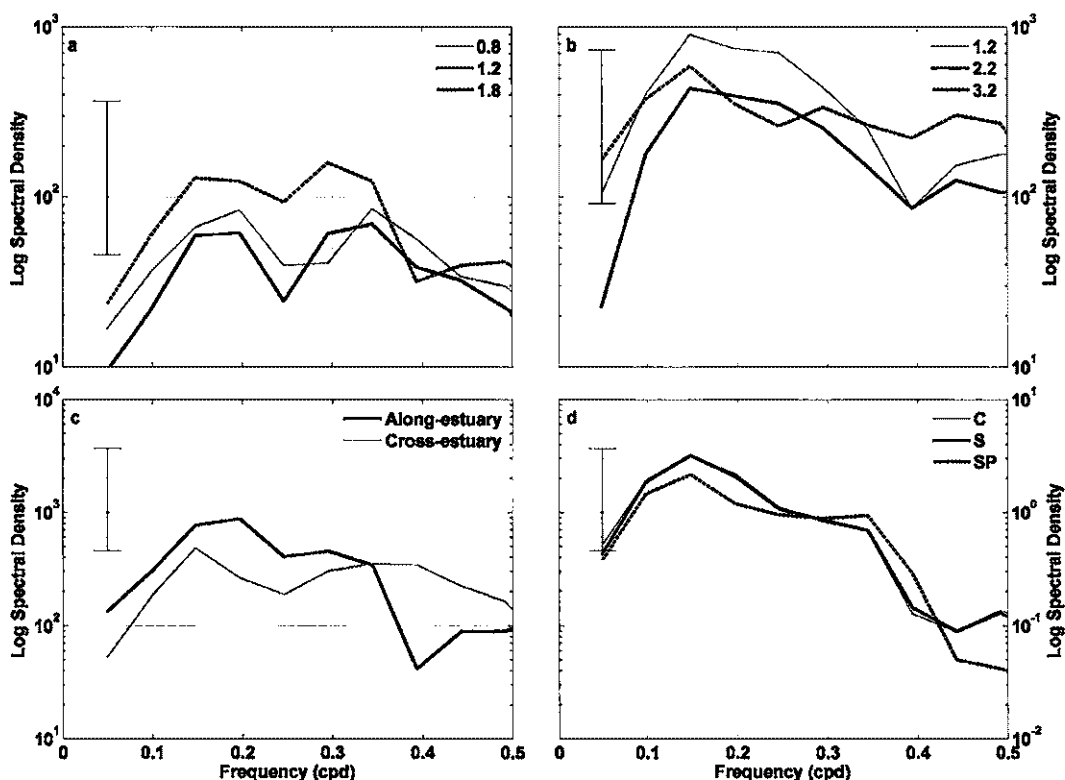


Fig. 12. Currents, wind and sea level spectral analysis for winter deployment. Along-channel flow (a) over the shoals, (b) in the channel, (c) wind components and (d) sea level at Sewells Point (SP) and bottom pressure in the channel (C) and over the shoals (S). Three representative depths were selected in order to show near the surface, middle and bottom current fluctuations. Depths are represented as meters above the bottom (mab). Vertical lines in each panel represent the 95% significant level.

Synoptic variability (3-7 days) was also apparent for the summer deployment over the shoal (Fig. 13a). In the channel a significant frequency of ~ 0.19 cpd (5 days) was

observed (Fig. 13b). In summer, contrasting the winter deployment, wind and sea level showed low spectral energy and no frequencies with significant energy (Fig. 13c, d). A wide frequency band was observed between 0.34 (3 days) and 0.14 cpd (7 days) for wind and between 0.25 (4 days) and 0.07 cpd (14 days) for sea level.

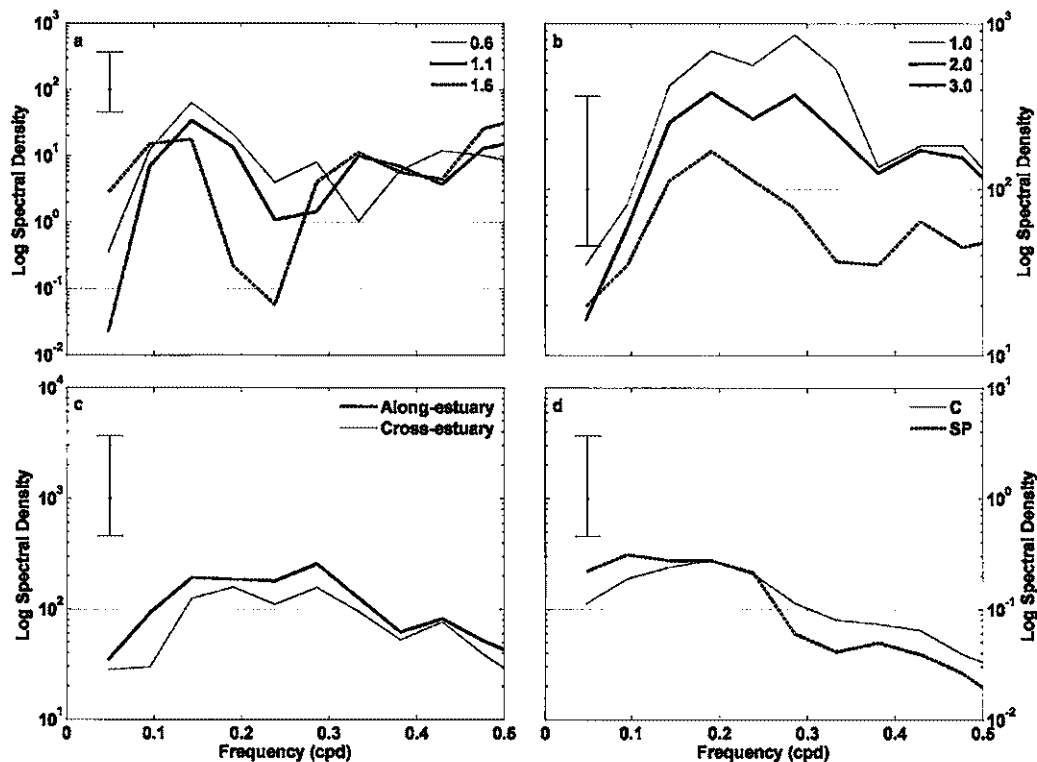


Fig. 13. Same as Fig. 12 but for the summer deployment.

The differences in the significant periods found between wind and sea level during the winter and summer deployments were also observed in the coherence and phase spectra (Fig. 14, 15, 16). Significant coherences between along-estuary wind and

the sea level at the entrance of the subestuary appeared between 0.34-0.1 (3-10 days) and 0.42-0.5 cpd (<2 days), with phases around 150° (Fig. 14a, b). During the summer deployment similar results were found, and again no significant coherence appeared between the along-estuary wind and the sea level at Sewells Point at periods longer than 2 days (Fig. 14c, d)

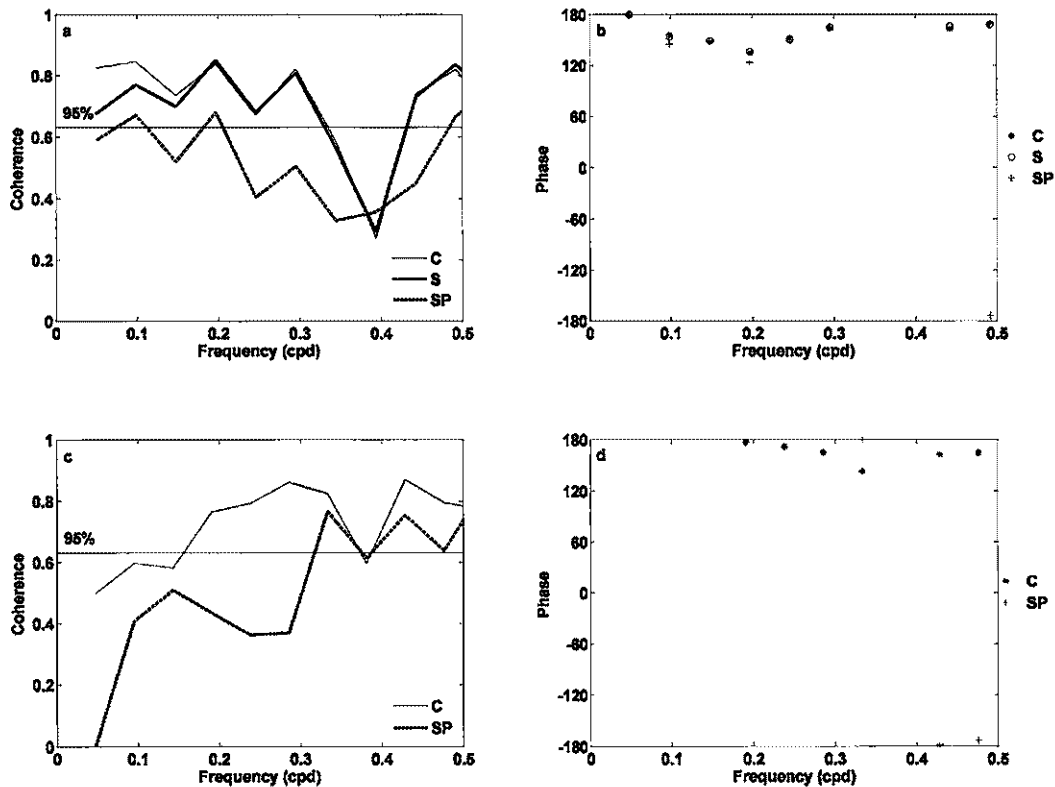


Fig. 14. Coherence and phase spectra between along-estuary wind and sea level at Sewells Point (SP) and bottom pressure in the channel (C) and over the shoal (S) for (a,b) winter and (c,d) summer deployments.

During winter, the coherence spectra between current and both the along-estuary wind and sea level (channel and shoal) showed good agreement at synoptic scales (3-7

days and ~ 2 days). In the channel significant coherence between current and along-estuary wind was found around 0.1-0.26 cpd (4-10 days) at all depths (Fig. 15a). Flow was also coherent with sea level at a period of 7 days (0.14 cpd), mostly at the surface layer (Fig. 15b). Over the shoals currents and wind were coherent throughout the water column at all frequencies (Fig. 15c). Current and sea level presented significant coherence in the entire water column at frequencies between 0.19 and 0.36 cpd (5-3 days) (Fig. 15d). During summer significant coherences between currents and wind were observed in the entire water column at all the frequencies > 0.1 cpd (Fig. 15e). Current and sea level also showed significant coherence at all depths between 3-7 days (Fig. 15f).

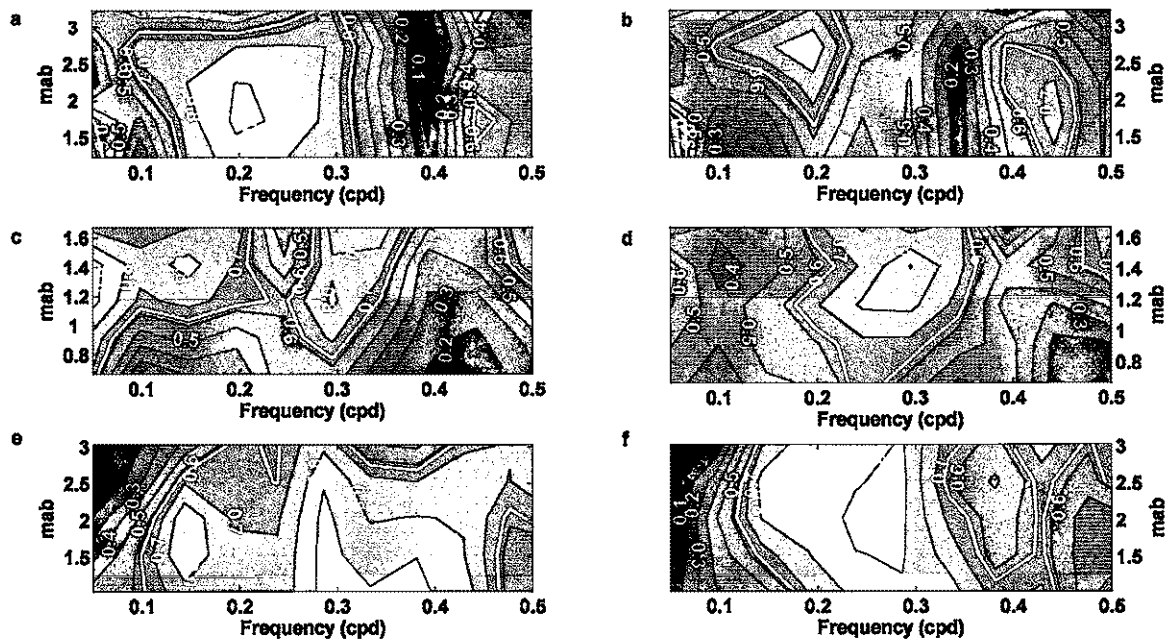


Fig. 15. Coherence spectra contours between: winter along-channel flow in the channel and, (a) along-estuary wind, (b) bottom pressure in the channel. Winter along-channel flow over the shoals and (c) along-estuary wind and (d) bottom pressure over the shoals. Summer along-channel flow in the channel and (e) along-estuary wind and (f) bottom pressure in the channel. White contour represent significant level and light gray correspond to high coherence values.

The phases for the currents and wind showed differences of almost 180 degrees in the channel (Fig. 16a) whereas the phase over the shoals was around -20 degrees (Fig. 16c) indicating negative relationship between the along-estuary flow and the along-estuary wind in the channel and positive relationship over the shoals. The reverse occurs between current and sea level since there is an opposite relationship between wind and sea level (Fig. 16b, d). In summer the phase in the channel was between -50 and 0 degrees among current, wind and sea level (Fig. 16e, f).

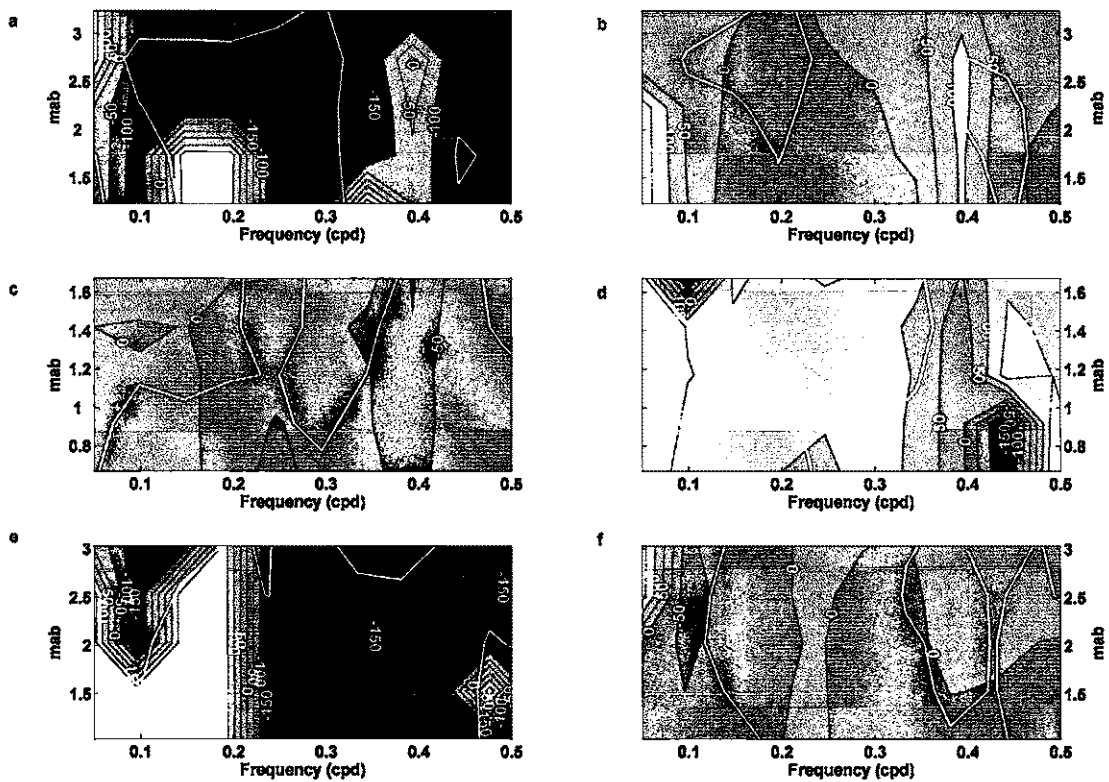


Fig. 16. Same as Fig. 15 but for phase spectra.

4.2.3 Empirical orthogonal functions

The first mode of the empirical orthogonal functions (1st EOF) explained more than 75% of the variability of the currents in both deployments and locations (Table 4), and showed a unidirectional vertical structure (Fig 17). For the winter deployment, fluctuations of the 1st EOF in the channel and over the shoal were followed negatively and positively by the winds, respectively (Fig. 17a). This mode was well correlated with the along-estuary wind; significant negative correlations ($r = -0.6$, $p < 0.05$) were found over the channel and positive correlations over the shoal ($r = 0.73$, $p < 0.05$). Similar results were found for the summer deployment (Fig. 17b), negative correlations ($r = -0.6$, $p < 0.05$) were observed in the channel but no significant correlations were observed over the shoals between currents and both wind components. The negative correlation between along-estuary wind and along-channel currents over the shoal for the summer (inverse to the winter correlation) does not represent the real effect of the wind over the current. This is likely a consequence of the shortness of the record over the shoal.

Table 4

Percentage explained for the first three EOF modes for each deployments and location at the entrance of the Nansemond River.

Mode	Winter		Summer	
	Channel	Shoal	Channel	Shoal
1	75.9	78.9	82.3	94.2
2	21.9	16.1	15.9	4.8
3	1.9	4.5	1.6	0.6

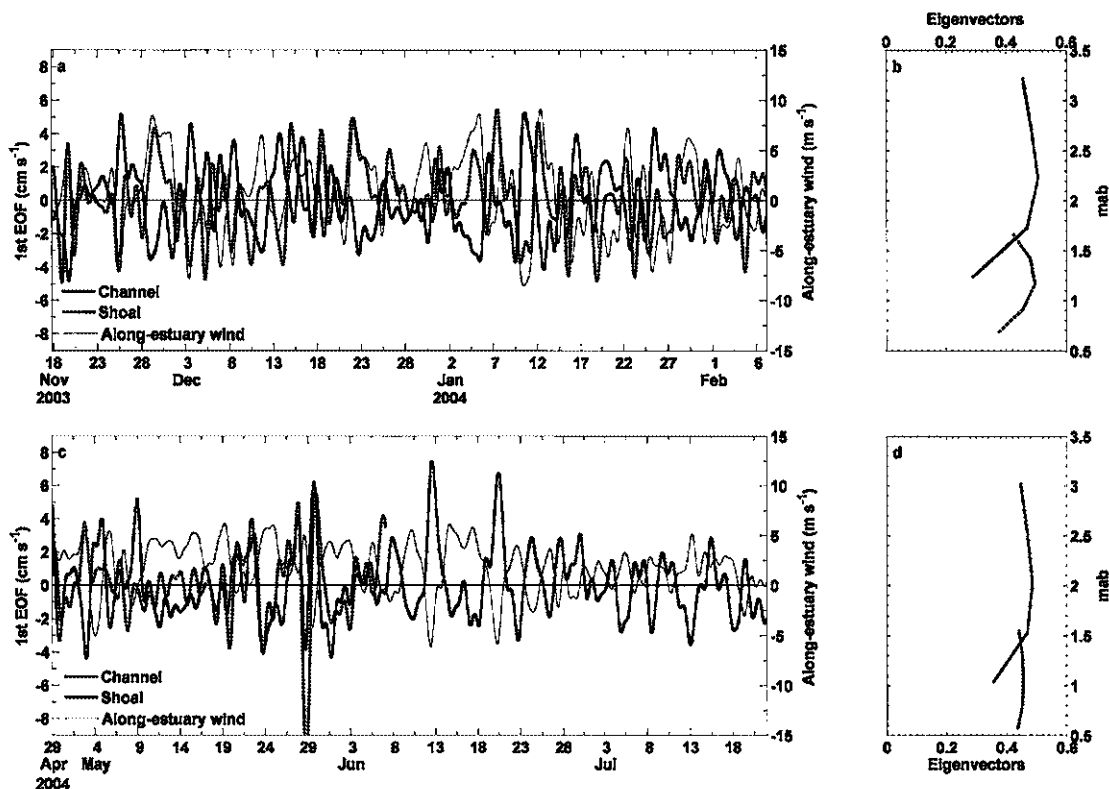


Fig. 17. First mode of empirical orthogonal functions (EOF) of (a) winter and (c) summer deployment. Right panels correspond to the vertical eigenvectors values for (b) winter and (d) summer periods.

The second EOF (2nd EOF) explained between 5 and 20% of the current variability depending of the deployment and location (Table 4). The eigenvectors of the 2nd EOF showed a bidirectional vertical structure (Fig. 18) for all the locations and periods. During winter, in the channel and over the shoals, the temporal variations of the 2nd EOF showed similarities with the vertical shear of along-channel flow, calculated as the difference between surface and bottom flow divided by the depth (Fig. 18a, b). Significant negative correlations ($r > 0.8$, $p < 0.05$) were observed between the two series

at both locations, suggesting that this mode was well represented by the estuarine circulation, i.e., surface outflows and bottom inflows. Similar results were observed for the summer period (Fig. 18c, d), with correlation over 0.7. In summary, this analysis suggest that the first EOFs, which explain more than 75% of the total variance is explained by the wind-driven variability. The second EOF is the estuarine circulation.

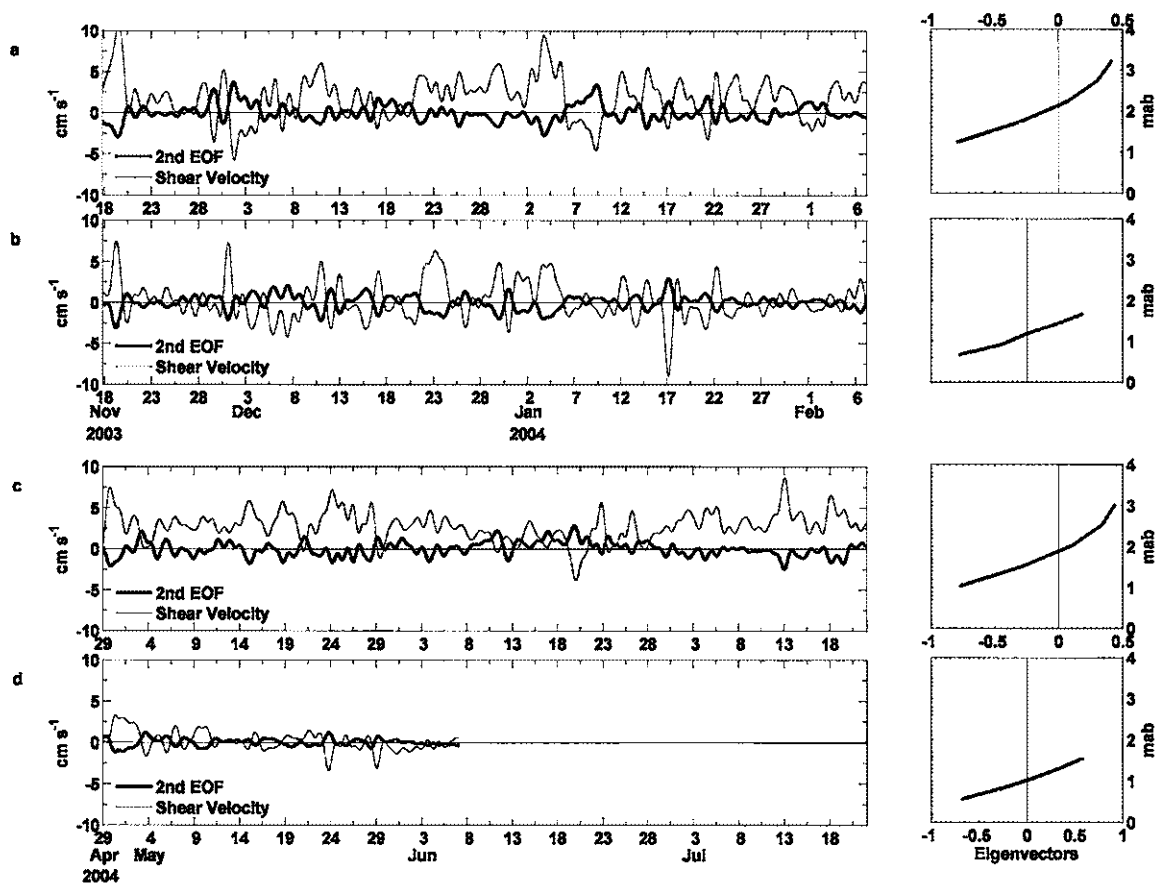


Fig. 18. Second mode of EOF for: Winter, (a) channel and (b) shoals. Summer, (c) channel and (d) shoals. Right panels are vertical eigenvectors values.

CHAPTER 5

DISCUSSION

Four oceanographic surveys and two periods of moored data were analyzed in order to study the subtidal exchange dynamics between a subestuary (Nansemond River), and its adjacent estuary (James River). The combination of both data sets allowed a characterization of the spatial and temporal variability of the subtidal circulation. The dynamics of the circulation may be described with a simple scaling of the momentum equation across the subestuary (1) and along the subestuary (2):

$$u \frac{\partial u}{\partial x} + v \frac{\partial u}{\partial y} + w \frac{\partial u}{\partial z} - fv = -\frac{1}{\rho} \frac{\partial P}{\partial x} + \frac{\partial}{\partial z} \left[A\nu \frac{\partial u}{\partial z} \right] \quad (1)$$

$$u \frac{\partial v}{\partial x} + v \frac{\partial v}{\partial y} + w \frac{\partial v}{\partial z} + fu = -\frac{1}{\rho} \frac{\partial P}{\partial y} + \frac{\partial}{\partial z} \left[A\nu \frac{\partial v}{\partial z} \right], \quad (2)$$

where u , v , w , are the across-channel, along-channel and vertical velocity components respectively. P is the pressure, f is the coriolis parameter, ρ is the density, $A\nu$ is the horizontal eddy viscosity coefficient and, x , y and z are the reference axis. The scaling shown in Table 5 is a result of the complex circulation patterns shown by the results described in previous chapter. This scaling shows that advections terms are important in the dynamics. The value of $A\nu$ was chosen according to previous estimations made by Valle-Levinson et al., 2000, in the James River estuary. In that study the authors found that, in general, the tidally averaged eddy viscosity value was $> 5 \times 10^{-4} \text{ m}^2 \text{ s}$. Therefore, for the purpose of the scaling presented here a value of $A\nu = 5 \times 10^{-4} \text{ m}^2 \text{ s}$, thus the scaled frictional term will represent the minimum value that this term would attain.

Table 5

Momentum equation scaling during each cruise for T1. Values ($\times 10^{-7}$) were estimated using mean velocities (U,V) for each cruise as shown in the last two column. $f = 8.7 \times 10^{-5} \text{ s}^{-1}$; $L_x = 1 \times 10^3 \text{ m}$; $L_y = 2 \times 10^2 \text{ m}$; $L_z = 2 \text{ m}$.

	Cross-channel scaling				Mean velocities (m s^{-1})	
	U^2/L_x	VU/L_y	fV	$A_v U/L_z^2$	U	V
N1	3.8	3.4	3.0	24	0.020	0.004
N2	0.7	11	23	10	0.008	0.027
N3	0.3	1.6	5.3	6.4	0.005	0.006
N4	0.2	3.5	14	5.4	0.004	0.016
	Along-channel scaling					
	UV/L_x	V^2/L_y	fU	$A_v V/L_z^2$		
N1	0.7	0.6	17	4.4		
N2	2.2	36	7.0	33		
N3	0.3	1.9	4.4	7.6		
N4	0.7	13	3.7	20		

Most of the terms were estimated with mean data available for each survey, except for the total pressure gradient. Advective terms (or centripetal accelerations), frictional effects and Coriolis accelerations have similar order of magnitude in all surveys. All of these terms contribute to balance the pressure gradient independently of spring and neap tidal forcing. Modulation of frictional accelerations and pressure gradients are expected to have a fortnightly period, i.e., the last term in eq. 1 and 2 should differ between spring and neap tides. Table 5 shows that this is unlikely, although small differences are observed. The along and across estuary baroclinic pressure gradient ($g/\rho_r \int_{-h}^z \frac{\partial \rho}{\partial x} dz$ and $g/\rho_r \int_{-h}^z \frac{\partial \rho}{\partial y} dz$, respectively) might be estimated using the available CTD casts for each survey. Similar to the frictional term and contrasting with the observations by Valle-Levinson et al. 2000, the baroclinic pressure gradient does not change appreciably among surveys (Table 6). A significant change occurs only when fresh water

intrusions enhance the transverse baroclinic pressure gradient but decrease the along estuary baroclinic pressure gradient (N2). Therefore, fortnightly variability seems not to play a role in the changes in stratification, and in subtidal flow.

Table 6

Baroclinic pressure gradients estimated with available CTD data. Values ($\times 10^{-7}$) were estimated using the differences in density between T1 and T3 integrated in 4m depth, with values of $g=9.8 \text{ m s}^{-2}$ and $\rho_r=1007 \text{ kg m}^{-3}$.

Survey	$g/\rho_r \int_{-h}^z \frac{\partial \rho}{\partial x} dz$	$g/\rho_r \int_{-h}^z \frac{\partial \rho}{\partial y} dz$
N1	11.45	21.6
N2	32.81	5.2
N3	14.63	28.5
N4	9.93	10.8

The main finding of this study is the recirculation area observed at the Nansmond River entrance, which may be the reason for the variations found in the present results compared to previous studies. Three aspects seem to reveal the presence of the recirculation. First, the subtidal flow shows no evidence of flow acceleration up the subestuary as might be expected for a Bernoulli-type circulation through a constriction. Second, the volume flux analysis shows disparate estimates among transects. Although roughly 25-50% of area was not covered by the measurements, the results show that, at least between T1 and T2, the lack in volume flux cannot be explained by the unmeasured area. Third, the scaling of the momentum equations shows that advections terms are important in the dynamics. All these three aspects suggest that the inflow is returning at some area of the lower Nansmond River causing the recirculation area. These results are consistent with recent work by Shen and Lin (2006). They determined the effects of tides

and stratification on the age of water in the James River by using a numerical model. Despite their purpose, which was not to study of the circulation patterns found in the model, the solution showed a recirculation area at the entrance to the Nansemond River (see Fig. 6 in Shen and Lin, 2006), which was derived from a 29-day vertically averaged flow.

The different conditions of wind, river discharge and tide among the oceanographic surveys and Shen and Lin's work, suggest that the morphology of the subestuary, a curved funnel, plays an important role in generating and maintaining the recirculation. Therefore, the recirculation would be a permanent characteristic of this subestuary. For a simple funnel shape, intensification of a Bernoulli-type flow would be expected in the narrow section, as shown in Fig. 19a.

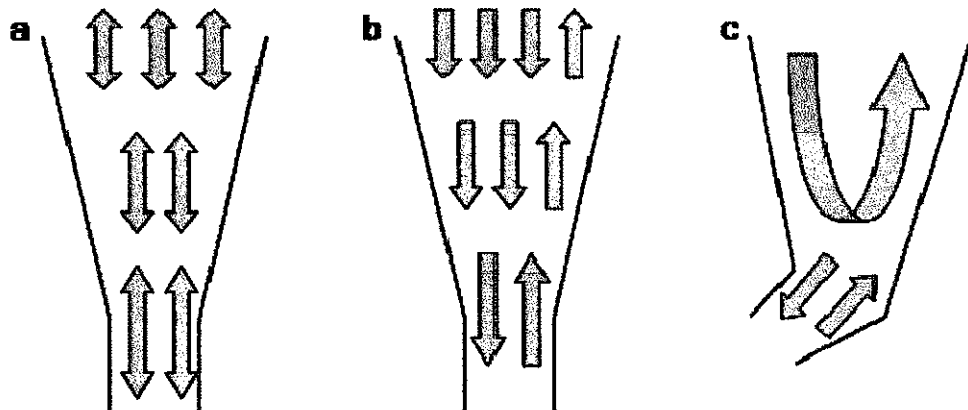


Fig. 19. Hypothetical representation of (a) Bernoulli circulation in a simple funnel, (b) circulation in an estuary-like funnel, and (c) the circulation pattern observed in this study as a result of a curved funnel shape of the subestuary.

Considering the transverse partition typically found in partially mixed and shallow estuaries, affected by the interaction of the transverse bathymetry with Coriolis and friction, a more realistic case would be similar to Fig.19b (outflow in the channel and inflows over the shoals at the entrance to the estuary). Stronger currents would still be expected in the narrow area. If the narrow area of the estuary is curved the result might be similar to the observations of this research and the flow might produce a recirculation (Fig. 19c).

The surveys show that the flow's return is enhanced when waters with lower salinity than up subestuary appear over the shoals at the entrance to the Nansemond River. The low salinity waters generate cross-channel salinity gradients and lateral circulation as well as unidirectional outflow in the channel. Although in the time series (see temporal variability section) this relationship is not especially apparent, a significant correlation does appear between the estuary discharge and the subestuary salinity. This suggests that only sporadic episodes of increase in the river discharge could lead to changes in the salinity and circulation as shown in N2. Thus, the estuary (James River) might play a crucial role in driving buoyancy forcing and pressure gradients in the subestuary (Nansemond River) when river discharge increases. These effects might be augmented by the fact that outflows in the James River occur on the left (south) shore (looking into the James River), i.e., the same side where the Nansemond River entrance is located as shown by Valle-Levinson et al. (2000). Therefore, an increase in the estuary discharge will be more perceptible at the entrance to the subestuary. Changes in transverse variability and general circulation of the estuary could also affect the dynamics in the subestuary and the sense of rotation of the recirculation. The unidirectional outflow

in the channel appeared only under the intrusion of fresh waters in the surveys. However, the temporal variability of the currents over the shoal and in the channel revealed that this pattern should occur more often than just under increased river discharge.

Correlation, spectral and EOF analyses show that wind is an important forcing of the subestuary circulation and the unidirectional flow in the channel. Also the importance of the wind can be observed in the large values of the frictional terms estimated in the momentum equation scaling (Table 5). For instance, more than 75% of the subtidal variance of the circulation can be explained by wind forcing especially the along-estuary wind. As previous studies of wind-induced exchange, predominant synoptic wind (3-10 days) drives currents and sea level causing the same scale of variability (Wong and Garvine, 1984; Garvine, 1985). Wong and Valle-Levinson (2002) found better relationships between wind, currents and sea level in autumn than in spring. The authors pointed out that this seasonality would depend on the frequency of the wind and the degree of stratification in the estuary. In our study area, minor differences occur between wind, currents and sea level from winter to summer. Stratification does not differ considerable year around, but wind fluctuations are indeed more energetic in winter than in summer (see Figs. 12c and 13c).

The relationship between wind and sea level could suggest a remote effect of the wind over the study area, i.e., a sea level set up or set down caused by the wind. However, under that scenario, a unidirectional volume exchange throughout the cross-estuary axis should occur (Wang, 1979a,b; Wong, 1994; Wong and Valle-Levinson, 2002). The results show a marked transverse partition instead of a unidirectional flow in the entire entrance to the subestuary. Even though the sea level responds as expected, up-

estuary (down-estuary) wind inducing a sea level set-up (set-down) along the entrance of the subestuary, the cross-channel variability of the flow reveals that local wind forcing should be more important than remote wind forcing (Wong and Moses-Hall, 1998; Wong and Valle-Levinson, 2002). Also the coherence spectra are more significant between the wind and the sea level at the entrance of the subestuary than the sea level at Sewells Point (same location where the wind was measured). This suggests that the wind has a direct effect over the sea level in the subestuary, while the variations of the sea level in the large estuary are not driven by the same local wind.

In the Nansemond River, up-estuary wind causes downwind flow over the shoals and upwind flow in the channel. Similar results have been shown by Wong (1994) and Sanay and Valle-Levinson (2005), to explain transverse variability in estuaries. However, only some studies (Valle-Levinson et al., 2001) have previously shown the same pattern using observational data. Therefore the results obtained in this study about exchange hydrodynamics of a subestuary, are among few that confirm the results of numerical models by using observational data. The transverse partition presented here, differs from previous studies of density-induced flows, which have shown inflow in channels and outflows over shoals (e.g., Kasai et al., 2000, Valle-Levinson et al., 2000; Valle-Levinson et al., 2001; Valle-Levinson et al., 2003). This discrepancy can be attributed to the greater influence of the local wind over density gradients, modifying the transverse partition previously described.

The recirculation revealed in this study might have important implications in pollution and ecology issues like larval retention and transport. In the past years, eutrophication (high levels of nutrients and primary production and, therefore, production

of organic matter) has become an important issue in several estuaries (Blanton et al., 2003; Kiddon et al., 2003; Kirby and Miller, 2005). Eutrophication has been caused mainly by anthropogenic factors like the increase in human population surrounding many estuaries combined with physical factors like poor water circulation and exchange. A recirculation zone at the entrance of any estuary further reduces the water exchange and increases the amount of time that contaminated and low oxygen waters remain inside the estuaries favoring conditions for eutrophication. Further, it is well known that retention of organisms and nutrients occurs in recirculation areas in estuaries (e.g., Sulkin 1981; Chen et al., 1997; Shen et al., 1999) as many organisms take advantage of the large quantities of food concentrated at these zones. Considering that around the Chesapeake Bay area there are many subestuaries with morphological features similar to those of Nansemond River, our results could be applied to them. Nevertheless, more studies and consideration of residence times and nutrient fluxes are crucial for a better understanding of the exchange dynamics between subestuaries and large estuaries and their effect on pollution and ecological problems.

CHAPTER 6

CONCLUSION

The major findings of this study about the exchange hydrodynamics between a subestuary and its adjacent estuary can be summarized as follows. (1) The circulation pattern observed in the subestuary is caused primarily by the interaction between local topography and local winds and secondarily by buoyancy forcing and Earth's rotation. Thus fortnightly tidal variability does not influence the dynamics of this subestuary. (2) The large estuary exerts influences controlling pressure gradients at the entrance of the subestuary through the intrusion of light waters during episodic increases of the estuary river discharge. The transverse variability and circulation pattern of the estuary also might have important effects in the dynamics of the subestuary but more studies are necessary to support this idea. (3) A subtidal recirculation seems to be a permanent feature of the subestuary caused by its curved funnel shape. This shape, instead of accelerating the flow as required by conservation of momentum, returns part of the flow and causes recirculation. (4) Enhancement of recirculation is caused by intrusion of less saline waters over the shoals of the subestuary and by westward wind, both of which generate a strong up subestuary flow and unidirectional outflow in the channel. (5) The transverse partition of the subtidal flows found in the subestuary is driven by winds. The observed downwind flows over the shoals (inflows) and upwind flows in the channel (outflows) show good agreement with analytical and numerical models, making this research one of the few studies to validate such numerical results.

REFERENCES

- Blanton, B.O., Seim, H.E., Alexander, C., Amft, J., Kineke, G., 2003. Transport of salt and suspended sediments in a curving channel of a coastal plain estuary: Satilla River, GA. *Estuarine, Coastal and Shelf Science* 75, 993-1006.
- Browne, D.R., Fisher, C.W., 1988. Tide and tidal currents in the Chesapeake Bay, U.S. Department of Commerce, Rockville, MD., 143 pp.
- Chen, C., Liu, H., Beardsley, R.C., 2003. An unstructured grid, finite-volume, three-dimensional, primitive equations ocean model: Application to coastal ocean and estuaries. *Journal of Atmospheric and Oceanic Technology* 20, 159-186.
- Chen, Y-H., Shaw, P-T., Wolcott, T.G., 1997. Enhancing estuarine retention of planktonic larvae by tidal currents. *Estuarine, Coastal and Shelf Science* 45, 525-533.
- Emery, W.J., Thomson, R.E., 1998. Data analysis methods in physical oceanography. Pergamon, New York, 632 pp.
- Friedrichs, C.T., Hamrick, J.M., 1996. Effects of channel geometry on cross-sectional variation in along channel velocity in partially stratified estuaries. In: Aubrey, D.G., Friedrichs C.T., (Eds.), *Buoyancy Effects on Coastal and Estuarine Dynamics*, AGU, Washington, D.C. pp. 283-300
- Garvine, R.W., 1985. A simple model of estuarine subtidal fluctuations forced by local and remote wind stress. *Journal of Geophysical Research* 90, 11,945-11,948.
- Geyer, W.R., 1993. Three-dimensional tidal flow around headlands. *Journal of Geophysical Research* 98, 955-966.

- Haas, L.W., 1977. The effect of the spring-neap tidal cycle on the vertical salinity structure of the James, York and Rappahannock Rivers, Virginia, USA. *Estuarine Coastal Marine Science* 5, 485-496.
- Hepworth, D., Kuo, A.Y., 1989. James River seed oyster bed project, Physical data report, I, 1984-1987, Virginia Institute of Marine Science, Gloucester Pt., VA.
- Joyce, T.M., 1989. On in situ calibration of shipboard ADCPs. *Journal of Atmospheric Oceanic Technology* 6, 169-172.
- Kasai, A., Hill, A.E., Fujiwara, T., Simpson, J.H., 2000. Effect of the Earth's rotation on the circulation in regions of freshwater influence. *Journal of Geophysical Research* 105, 16,961-16,969.
- Kiddon, J.A., Paul, J.F., Buffum, H.W., Strobel, C.S., Hale, S.S., Cobb, D., Brown, B.S., 2003. Ecological condition of US Mid-Atlantic estuaries, 1997-1998. *Marine Pollution Bulletin* 46, 1224-1244.
- Kirby, M.X., Miller, H.M., 2005. Response of a benthic suspension feeder (*Crassostrea virginica* Gmelin) to three centuries of anthropogenic eutrophication in Chesapeake Bay. *Estuarine, Coastal and Shelf Science* 62, 679-689.
- Li, C., O'Donnell, J., 1997. Tidally induced residual circulation in shallow estuaries with lateral depth variation. *Journal of Geophysical Research* 102, 27,915-27,929.
- Moon, C., Dunstan, W.M., 1990. Hydrodynamic trapping in the formation of the chlorophyll a peak in turbid, very low salinity waters of estuaries. *Journal of Plankton Research* 12, 323-336.

- Nunes, R.A., Lennon, G.W., 1987. Episodic stratification and gravity currents in a marine environment of modulated turbulence. *Journal of Geophysical Research* 92, 5465-5480.
- Officer, C.B., 1976. *Physical oceanography of estuaries (and associated coastal waters)*. John Wiley, New York, 465 pp.
- Paraso, M.C., Valle-Levinson, A., 1996. Meteorological influences on sea level and water temperature in the lower Chesapeake Bay: 1992. *Estuaries* 19, 548-561.
- Piñones, M.A., 2006. Tidally induced variability at the Chesapeake Bay entrance, M.S. Thesis. Department of Ocean, Earth and Atmospheric Sciences, Old Dominion University, unpublished.
- Pritchard, D.W., 1956. The dynamic structure of a coastal plain estuary. *Journal of Marine Research* 15, 33-42.
- Sanay, R., Valle-Levinson, A., 2005. Wind-induced circulation in semienclosed homogeneous, rotating basins. *Journal of Physical Oceanography* 35, 2520-2531.
- Shen, J., Boon, J.D., Kuo, A.Y., 1999. A modeling study of a tidal intrusion front and its impact on larval dispersion in the James River estuary, Virginia. *Estuaries* 22, 681-692.
- Shen, J., Lin, J., 2006. Modeling study of the influences of tide and stratification on age of water in the tidal James River. *Estuarine, Coastal and Shelf Science* 68, 101-112.
- Simpson, J.H., Brown, J., Matthews, J.P., Allen, G., 1990. Tidal straining, density currents and stirring in the control of estuarine stratification. *Estuaries* 12, 125-132.

- Sulkin, S., 1981. Larval retention in estuaries. *Estuaries* 4, 238-304.
- Uncles, R.J., 2002. Estuarine physical processes research: Some recent studies and progress. *Estuarine, Coastal and Shelf Science* 55, 829-856.
- Valle-Levinson, A., O'Donnell, J., 1996. Tidal interaction with buoyancy driven flow in a coastal plain estuary. In: Aubrey, D.G., Friedrichs C.T., (Eds.), *Buoyancy Effects on Coastal and Estuarine Dynamics*, AGU, Washington, D.C. pp. 256-281.
- Valle-Levinson, A., Li, C., Royer, T.C., and Atkinson, L.P., 1998. Flow patterns at the Chesapeake Bay entrance. *Continental Shelf Research* 18, 1157-1177.
- Valle-Levinson, A., Atkinson, L.P., 1999. Spatial gradients in the flow over an estuarine channel. *Estuaries* 22, 179-193.
- Valle-Levinson, A., Wong, K.C., Lwiza, K.M.M., 2000. Fortnightly variability in the transverse dynamics of a coastal plain estuary. *Journal of Geophysical Research* 105, 3413-3424.
- Valle-Levinson, A., Delgado, J.A., Atkinson, L.P., 2001. Reversing water exchange patterns at the entrance to a semiarid coastal lagoon. *Estuarine, Coastal and Shelf Science* 53, 825-838.
- Valle-Levinson, A., Reyes, C., Sanay, R., 2003. Effects of bathymetry, friction, and rotation on estuary-ocean exchange *Journal of Physical Oceanography*, 2375-2393.
- Wang, D.P., 1979a. Wind-driven circulation in the Chesapeake Bay, winter 1975. *Journal of Physical Oceanography* 9, 564-572.
- Wang, D.P., 1979b. Subtidal sea level variations in the Chesapeake Bay and relations to atmospheric forcing. *Journal of Physical Oceanography* 9, 413-421.

- Winant, C.D., 2004. Three-dimensional wind-driven flow in an elongated, rotating basin. *Journal of Physical Oceanography* 34, 462-476.
- Wong, K.C., Garvine, R.W., 1984. Observations of wind-induced, subtidal variability in the Delaware estuary. *Journal of Geophysical Research* 89, 10,589-10,597.
- Wong, K.C., 1994. On the nature of transverse variability in a coastal plain estuary. *Journal of Geophysical Research* 99, 14,209-14,222.
- Wong, K.C., Moses-Hall, J.E., 1998. On the relative importance of the remote and local wind effects on the subtidal variability in a coastal plain estuary. *Journal of Geophysical Research* 103, 18,393-18,404.
- Wong, K.C., 2002. On the wind-induced exchange between Indian River Bay, Delaware and the adjacent continental shelf. *Continental Shelf Research* 22, 1651-1668.
- Wong, K.C., Valle-Levinson, A., 2002. On the relative importance of the remote and local wind effects on the subtidal exchange at the entrance to the Chesapeake Bay. *Journal of Marine Research* 60, 477-498.

VITA

Diego A. Narváez

Education

- 2000 B. S. Oceanography. Pontificia Universidad Católica de Valparaíso, Valparaíso, Chile.
- 2006 M. S. Ocean and Earth Science. Center for Coastal Physical Oceanography. Department of Ocean, Earth and Atmospheric Sciences, Old Dominion University, Norfolk, Virginia, USA.

Experience

- 1996-1999 Research assistant. Physical Oceanography Laboratory, Pontificia Universidad Católica de Valparaíso, Valparaíso, Chile.
- 2000-2004 Research assistant. Estación Costera de Investigaciones Marinas (ECIM), Pontificia Universidad Católica de Chile, Las Cruces, Chile.
- 2005-2006 Research assistant. Center for Coastal Physical Oceanography (CCPO), Old Dominion University, Norfolk, Virginia, USA.

Publications

- Vargas, C.A., Narváez, D.A., Piñones, A., Navarrete, S.A., Lagos, N.A., 2006. River plume dynamic influences transport of barnacle larvae in the inner shelf off central Chile. *Journal of the Marine Biological Association UK*, 86, 1057-1065.
- Narváez, D.A., Navarrete, S.A., Largier, J.L., Vargas, C.A., 2006. Onshore advection of warm water, larval invertebrate settlement, and relaxation of upwelling off central Chile. *Marine Ecology Progress Series*, 309, 159-173.
- Piñones, M.A., Valle-Levinson, A., Narváez, D.A., Vargas, C.A., Navarrete, S.A., Yuras, G., Castilla, J.C., 2005. Wind-induced diurnal variability in river plume motion. *Estuarine Coastal and Shelf Science*, 65(3), 513-525.
- Vargas, C.A., Narváez, D.A., Piñones, A., Venegas, R.M., Navarrete, S.A., 2004. Internal tidal bore warm fronts and settlement of invertebrates in central Chile. *Estuarine Coastal and Shelf Science*. 61(4), 603-612.
- Narváez, D.A., Poulin, E., Leiva, G., Hernández, E., Castilla, J.C., Navarrete, S.A., 2004. Seasonal and spatial variation of nearshore hydrographic conditions in central Chile. *Continental Shelf Research*, 24(2), 279-292.
- Poulin, E., Palma, A.T., Leiva, G., Narváez, D.A., Navarrete, S.A., Castilla, J.C., 2002. Avoiding offshore transport of competent larvae during upwelling events: The case of the gastropod *Concholepas concholepas* in central Chile. *Limnology & Oceanography*, 47(4), 1248-1255.